3D Printing Technologies for Electrochemical Energy Storage

Feng Zhang, Min Wei, Vilayanur V Viswanathan, Benjamin Swart, Yuyan Shao, Gang Wu, Chi Zhou

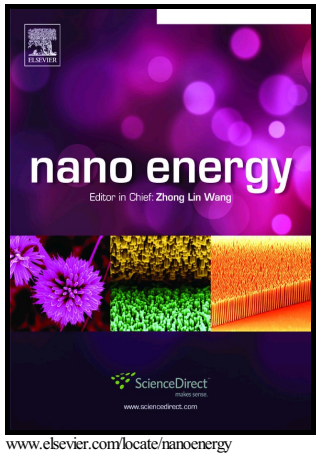

www.elsevier.com/locate/nanoenergy

PII: S2211-2855(17)30513-X
DOI: http://dx.doi.org/10.1016/j.nanoen.2017.08.037
Reference: NANOEN2151

To appear in: *Nano Energy*

Received date: 12 May 2017
Revised date: 14 August 2017
Accepted date: 20 August 2017

Cite this article as: Feng Zhang, Min Wei, Vilayanur V Viswanathan, Benjamin Swart, Yuyan Shao, Gang Wu and Chi Zhou, 3D Printing Technologies for Electrochemical Energy Storage, *Nano Energy,* http://dx.doi.org/10.1016/j.nanoen.2017.08.037

3D Printing Technologies for Electrochemical Energy Storage

Feng Zhang[a], Min Wei[b], Vilayanur V Viswanathan[c], Benjamin Swart[a], Yuyan Shao[c,*], Gang Wu[b,*], and Chi Zhou[a,*]

[a] Department of Industrial Engineering, University at Buffalo, The State University of New York, Buffalo, New York 14260, United States

[b] Department of Chemical and Biological Engineering, University at Buffalo, The State University of New York, Buffalo, NY 14260, United States

[c] Pacific Northwest National Laboratory, Richland, WA 99352, United States

Corresponding authors: yuyan.shao@pnnl.gov (Y. Shao), gangwu@buffalo.edu (G. Wu), chizhou@buffalo.edu (C. Zhou)

Abstract: Fabrication and assembly of electrodes and electrolytes play an important role in promoting the performance of electrochemical energy storage (EES) devices such as batteries and supercapacitors. Traditional fabrication techniques have limited capability in controlling the geometry and architecture of the electrode and solid-state electrolytes, which would otherwise compromise the performance. 3D printing, a disruptive manufacturing technology, has emerged as an innovative approach to fabricating EES devices from nanoscale to macroscale, providing great opportunities to accurately control device geometry (*e.g.*, dimension, porosity, and morphology) and structure with enhanced specific energy and power densities. Moreover, the "additive" manufacturing nature of 3D printing provides excellent controllability of the electrode thickness with much simplified process in a cost effective manner. With the unique spatial and temporal material manipulation capability, 3D printing can integrate multiple nano-materials in

the same print, and multi-functional EES devices (including functional gradient devices) can be fabricated. Herein, we review recent advances in 3D printing of EES devices. We focus on two major 3D printing technologies including direct writing and inkjet printing. The direct material deposition characteristics of these two processes enable them to print on a variety of flat substrates, even a conformal one, well suiting them to applications such as wearable devices and on-chip integrations. Other potential 3D printing techniques such as freeze nano-printing, stereolithography, fused deposition modeling, binder jetting, laminated object manufacturing, and metal 3D printing are also introduced. The advantages and limitations of each 3D printing technology are extensively discussed. More importantly, we provide a perspective on how to integrate the emerging 3D printing with existing technologies to create structures over multiple length scale from nano to macro for EES applications.

Keywords: 3D printing, electrochemical energy storage, inkjet printing, direct ink writing, nano printing.

Table of Contents

1. Introduction

Electrochemical energy storage (EES) devices such as batteries and supercapacitors play a key role in our society [1-4]. In the past two decades, the development of energy storage devices has attracted increasing interests among industry and academia. However, most of the academic research has been focused on the exploration of new electrode materials [5] and new electrolytes [6]; not enough attention has been paid to the fabrication process, which is the bridge to transfer materials to devices. While scientific discovery and materials innovation are important, process engineering on how to put these pieces of building block together plays a crucial, often determining role in real world devices [7-10].

Conventionally, electrode fabrication in research area mainly relies on various deposition techniques such as Meyer rod coating, spray deposition [11, 12], electrochemical deposition [13, 14], electrophoretic deposition [15, 16], sputtering [17, 18], chemical vapor deposition (CVD) [19, 20], atomic layer deposition (ALD) [21], layer-by-layer deposition (LbL) [22, 23], sol-gel [24, 25], and spin-coating [26]. These physical/chemical deposition methods provide versatile and facile routes to produce EES devices. However, their applications in practice for large-scale manufacturing and on-chip integration are limited by the complex material handling procedures,

special chemical bath requirement, and difficulty in controlling the thickness and uniformity thin film [27, 28]. In industry, traditional EES devices are fabricated through high speed roll-to-roll processing, which normally experiences chemicals deposition, electrode rolling, roll cutting, cell assembly with separator, electrolyte filling, and finally packaging with re-cutting. This intricate technology, adopted from magnetic tape factories in Japan in the 1980's and 1990's, takes a long time to produce a device and is limited in further scaling up fabrication other than making the production line longer. Highly compacted and automated manufacturing methods can greatly decrease the fabrication time and upfront investment [29]. Still, for the rapid development of the Internet of Things (IoT), the energy storage devices of the future are envisioned to be flexible, wearable, lightweight, on-chip integratable with other electronics, and delicate in size with various form factors and aesthetic diversity [30, 31]. In short, future power sources need to be customizable.

The rise of 3D printing, also known as additive manufacturing (AM) or solid freeform fabrication (SFF), offers a flexible, efficient, and economical maneuver to fabricate energy storage devices [32-34]. 3D printing refers to a wealth of techniques that fabricate an object layer by layer directly from a computer aided design (CAD) model without part-specific tooling. AM technologies can be categorized into the following seven types according to ASTM International [35]: (1) material extrusion (e.g. direct writing, fused deposition modeling), (2) powder bed fusion (e.g. selective laser sintering, direct metal laser sintering) (3) vat photopolymerization (e.g. stereolithography), (4) material jetting (e.g. PolyJet™, and other inkjet printing related processes), (5) binder jetting, (6) sheet lamination (e.g. laminated object manufacturing) , and (7) directed energy deposition (e.g. laser net shape engineering). Due to these versatile processes, 3D printing possess the potential to print electronics [36, 37], energy storage devices [32, 33],

ceramics and glasses [38-40], automotive and aircraft components [41, 42], artificial ears [43], prosthetic limbs [44], metamaterials [45, 46] and food [47], to name a few. In the past several years, multiple 3D printing techniques have been applied to fabricate EES devices, including direct ink writing (DIW) [32, 33, 48-57], inkjet printing (IJP) [31, 58-74], stereolithography (SLA®) [75, 76], fused deposition modeling (FDM®) [77-79], binder jetting (3DP™) [80], laminated object manufacturing (LOM™) and metal 3D printing [81-84].

Compared to conventional EES fabrication processes, 3D printing offers several advantages:

- 3D printing demonstrates excellent process flexibility and geometry controllability. 3D printing covers a wide spectrum of material from liquid solution, powder, filament, and laminate. These versatile forms could well facilitate the doping of favorable nanomaterials from zero-dimensional (0D) such as carbon coated nanoparticles, to one-dimensional (1D) such as carbon nanotubes, and to two-dimensional (2D) such as graphene. A comprehensive understanding of the EES fabrication processes with associated materials is shown in **Figure 1.** Very complex shaped devices can be readily realized by 3D printing. The complexity can be in planar and also in three dimensional (3D) space. Favorable interdigital patterns that require great effort to produce in conventional methods have been easily realized in a variety of 3D printing approaches [32, 54]. Particular space architectures with periodic or aligned pores enable fast ion transport which is beneficial for fast charge/discharge, and increased active material loading in the third dimension would greatly promote the energy storage.
- 3D printing can well control the thickness of electrodes because of the layer by layer additive manufacturing nature of 3D printing technology. Thin-film energy devices can be fabricated by just depositing material over a few layers, which are applicable for flexible, wearable devices. Very thick electrodes can also be printed, which can acquire promoted energy

density per foot area. In general, the precise layer-wise assembly feature of 3D printing allows the electrode thickness to be well controlled out of plane.

- The performance of 3D printed energy device typically outweighs their bulk counterparts. For instance, the areal energy and power density of the 3D micro battery is much higher than its rechargeable counterparts due to the direct writing technology used that enables the capability to fabricate high aspect structures within a small areal footprint [32]. Thanks to the 3D-printed macro-architecture that facilitates fast ion diffusion through the thick electrode, the rate capability of the printed three-dimensional, hierarchical graphene aerogel based supercapacitor electrode is among the highest compared to other reported carbon-based electrodes [33].
- 3D printing is cost effective and environment friendly. This is attributed to the much simplified process that enables one-step fabrication. 3D printing adopts the additive manufacturing strategy, meaning material is deposited on demand. This characteristic maximally eliminates material wastage, making it much more energy-conservative and environment-friendly than conventional methods.

Overall, 3D printing offers a completely new bottom-up manufacturing strategy to fabricate EES devices. In this review, we focus on reviewing various state-of-the-art 3D printing approaches to fabricate EES devices and their components.

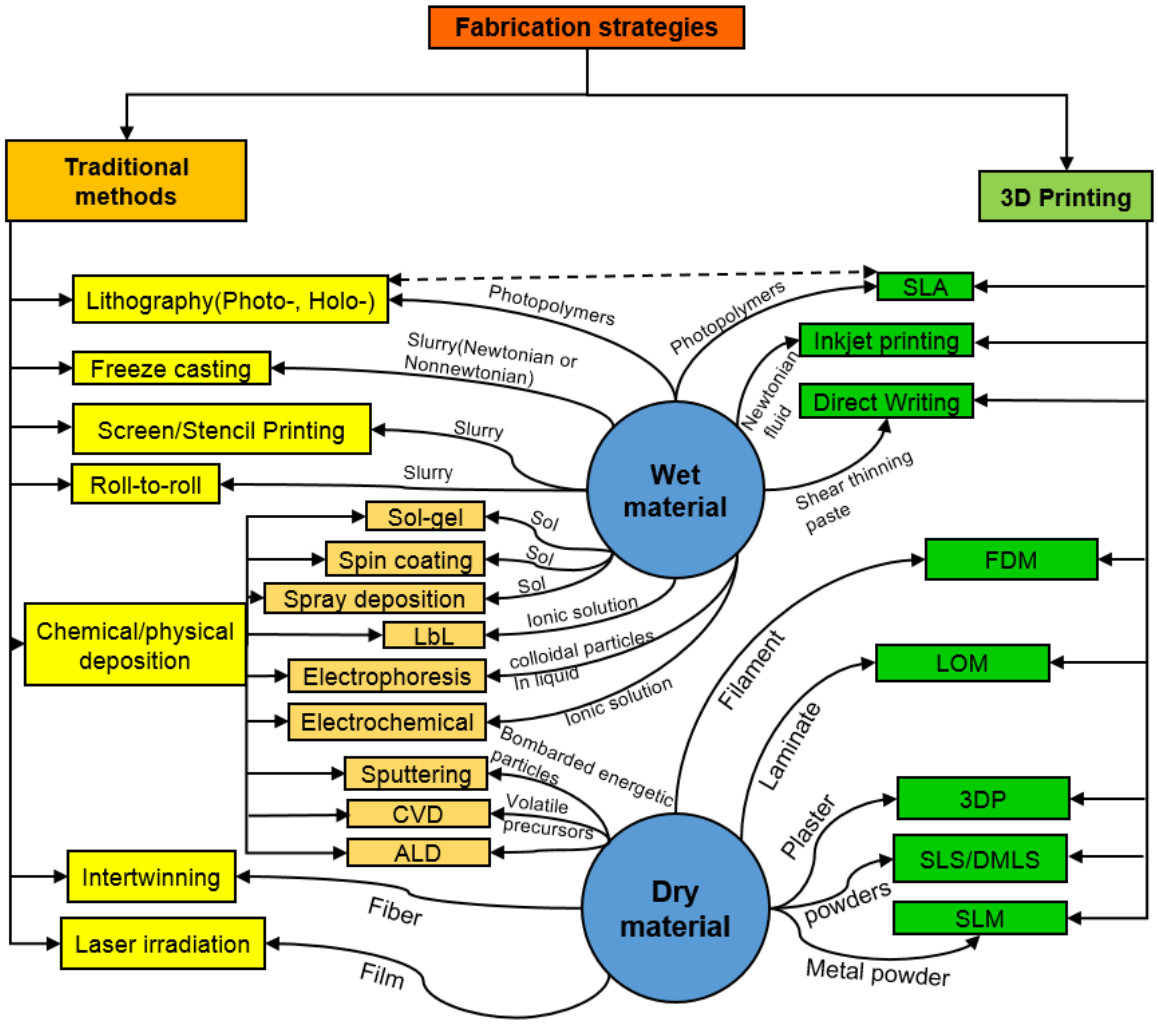

Figure 1. A systematic map showing the various processes and associated material types.

2. 3D printing for energy storage

The most widely used 3D printing techniques for EES are inkjet printing and direct writing. The traditional ink-like materials, which are formed by dispersing electrode active materials in a solvent, can be readily extended or directly used in these two processes. Other 3D printing processes may need special material engineering or process combination to be properly adapted.

The details of each process in electrochemical applications are elucidated in the following sections.

2.1 Inkjet printing (IJP)

IJP is a droplet-based material deposition process originally used for graphic or document printing in 2D space. As a promising technique, IJP is capable of producing complex patterns with high resolution and excellent multi-material printing capability. It has been developed as a non-contact, direct material deposition technology for various applications from electrical to biomedical [85]. In the field of 3D printing, IJP has been developed into two important processes: polymer jetting and binder jetting. In the polymer jetting process, the inkjet print head deposits photosensitive polymer that is cured by a light source upon landing onto the substrate; while in the binder jetting process, the binder is selectively ejected onto a powder bed to form a cross section of the object, which is known as 3DP. Because the liquid material used in IJP is quite similar to that used in typical conventional processes such as Meyer rod coating, together with the high resolution of inkjet technology with excellent multi-material printing capability, IJP is largely used for printing batteries [61, 62, 65, 68, 74] and supercapacitors [31, 58-60, 63, 66, 67, 69-71, 73]. Typically, to prepare the ink, active material is dispersed into a solvent. The formation of the final material used for IJP should be in a diluted liquid form. The ink for IJP must be well formulated without any agglomerate in order to avoid possible clogging during printing. Also, the active material loading in the ink cannot be high, otherwise the required ink with particular fluid behavior cannot be obtained. In general, the ink characteristics such as viscosity μ, surface tension σ and density ρ, must be within certain ranges and satisfy certain rules for a fixed nozzle diameter d to allow the inkjet process to work properly [86]. The inverse Ohnesorge number Z is commonly used to predict if a stable inkjet drop will be formed: $Z =$

$1/Oh = \sqrt{\rho d\sigma}/\mu$. Only if 1< Z<10, can the ink be expected to produce stable droplets. **Table 1** summarizes the various ink prescriptions in the literatures and the inkjet printer used for each specific work.

2.1.1 Inkjet-printed supercapacitors

Currently, electrode materials for supercapacitors include carbonaceous material, conductive polymers, and metal oxide. Carbon materials, such as activated carbons (ACs), carbon nanotubes (CNTs), and graphene, are mainly used as electrode material for electric double-layer capacitors (EDLC). Conductive polymer and metal composites are pseudocapacitance materials. Carbon-based material, due to its low cost, variety of forms, and excellent electrochemical stability [87], have been extensively utilized as an active material for supercapacitor electrode. However, as most carbon-based material is not hydrophilic, specific surfactant needs to be selected for the proper dispersion of active material in order to use them for IJP. In the case of CNTs, sodium dodecyl sulfate (SDS) and sodium dodecylbenzene sulfonate (SDBS) are commonly used [31, 58, 71].

ACs is one of the most popular electrode materials due to the large specific surface area (SSA) and good electrical property. ACs ink was used to fabricate interdigitated micro-supercapacitors using IJP [70]. The ink was prescribed by mixing activated carbon powder with a polytetrafluoroethylene (PTFE) polymer binder in ethylene glycol, and stabilized with a Triton X100 surfactant. The well prescribed ink was then deposited onto photolithography patterned gold (Au) interdigital current collectors, which were vapor deposited on a silica based substrate. **Figure 2b** shows a micro-supercapacitor inkjet printed with 20 fingers, 40 μm wide, and interspaced by 40 μm.

CNTs are also favorable electrode materials due to their excellent electrical conductivity and mechanical stability. Supercapacitors with inkjet-printed single-walled carbon nanotube (SWCNT) thin film electrodes were reported as well [58]. Due to the integration of ruthenium oxide nanowires, the knee frequency of the hybrid thin film was much higher than that of bare SWCNT electrode and the electrochemical performance was also significantly improved. Recently, a fully printable supercapacitor was demonstrated using a commercial desktop inkjet printer [31]. The supercapacitor, which was composed of activated carbon/ CNTs as electrodes and an ionic liquid/ultraviolet-cured triacrylate polymer-based solid-state electrolyte, could be printed into artistic patterns and connected in parallel to enhance the capacitance. This work represents the first fully printed, all-solid-state supercapacitor using IJP, as all components including electrode, electrolyte, current collector, and even substrate are inkjet-printed.

Due to the abundant oxygen-containing functional groups [88], graphene oxide (GO) and partially reduced GO (rGO) can be readily dispersed with water, and then used for inkjet printing. The aqueous GO solution is an ideal candidate material for inkjet based 3D printing processes [66, 67, 89]. After printing, the GO structure can be thermally reduced to obtain conductive graphene electrode [63]. Doping pseudocapacitance material into EDLC material could potentially elevate the total capacitance of device as explained previously. Conductive polymer is commonly used as electrode material for Pseudocapacitors. The most popularly used conductive polymers include polypyrrole (PPy), poly (3, 4-ethylenedioxythiophene) polystyrene sulfonate (PEDOT: PSS), and polyaniline (PANI). To promote the capacitance, nano graphene platelets/polyaniline (NGP/PANI) hybrid ink was formulated to prepare thin-film electrodes [73]. An inkjet-printed flexible all-solid-state symmetric supercapacitor based on GH−PANI/GP electrode and gel electrolyte was also reported [59]. As shown in **Figure 2c**, the GO ink was first

deposited onto a paper substrate to form the GO based paper substrate (GOP). The well prescribed graphene hydrogel/PANI ink was then deposited onto the GOP substrate to obtain the electrode structure. The assembled supercapacitor using gel electrolytes exhibited remarkable mechanical flexibility, high cycling performance.

Apart from the above mentioned carbon-based materials, researchers also explored other materials for inkjet printing of supercapacitors. For example, lamellar potassium cobalt phosphate hydrate nanocrystal whiskers was used to print the first flexible all-solid-state asymmetric micro-supercapacitor [69]. The micro device showed excellent mechanical and electrical properties due to the highly-interconnected layer structure. Inkjet-printed polyimide films could work as dielectric materials for microelectronic applications [90]. The film was formed with poly(amic) acid printed on to a hot substrate (around 160 ^{o}C) to initialize a rapid thermal imidization.

In short, IJP enables to deposit a variety of carbon-based material for EDLC fabrication with designed pattern directly from a CAD file. This process only requires the suitable Newtonian fluid ink to be well defined. However, since most processes have the solvent removed in an evaporation manner, the capability to print very thick electrode is limited by the elevated built time.

2.1.2 Inkjet-printed batteries

Lithium-ion batteries (LIBs) play a critical role in the consumer rechargeable battery market. Some pioneering work using IJP to fabricate lithium-ion thin film electrode involves various metal oxide inks. MnO_2, SnO_2, and $LiCoO_2$ (LCO) thin film electrodes were printed using inkjet technologies [65, 72, 74]. Recently, IJP of carbon coated $LiFePO_4$ (LFP) material was also demonstrated [61, 62]. The coated carbon on LFP could greatly improve the conductivity of

electrodes. Due to the high porosity and thin film characteristics of electrodes realized by IJP, very high rate capability is achieved. However, it remains unknown how the high porosity is achieved through IJP.

Ho *et al.* reported the first inkjet-printed zinc-silver 3D microbattery using electrohydrodynamic (EHD) technology [64]. The EHD technique utilized allowed the droplets to be as small as one femtoliter, which enabled producing of lateral feature sizes in the sub-micron scale. The electrode was prepared by printing sparse silver pillars on silver pads, and then submerged into KOH with dissolved ZnO powder. The patterned sliver array 3D electrodes acquired an energy density of 3.95 mWh/cm^2, which is much higher than the planar counterpart. It is interesting to know that only 2.5% of the electrode footprint area was used for patterning pillars. We believe that with a much denser array of pillars and higher aspect ratio, much higher capacities could be obtained.

Recently, inkjet-printed Lithium-sulfur (Li-S) batteries have also been reported. To prepare the ink, SWCNT with 95% metallic content was infused with sulfur, and dispersed in Cumene hydroperoxide (CHP). Compared to Li-ion battery, Li-S batteries could achieve much higher specific energy [91]. The fabricated battery delivered a capacity of 850 mAh/g-sulfur which was the highest among the inkjet printing fabricated batteries so far [68]. It should be noted that the concentration of active material used for inkjet printing is only 0.2 mg/ml. We believe that with a much higher material loading, the performance would be further improved.

In conclusion, owing to the high precision patterning capability and rich material selections, inkjet offers great potential to engineer the structure of electrode in very accurate manner, which can improve the rate capability and areal energy density of batteries.

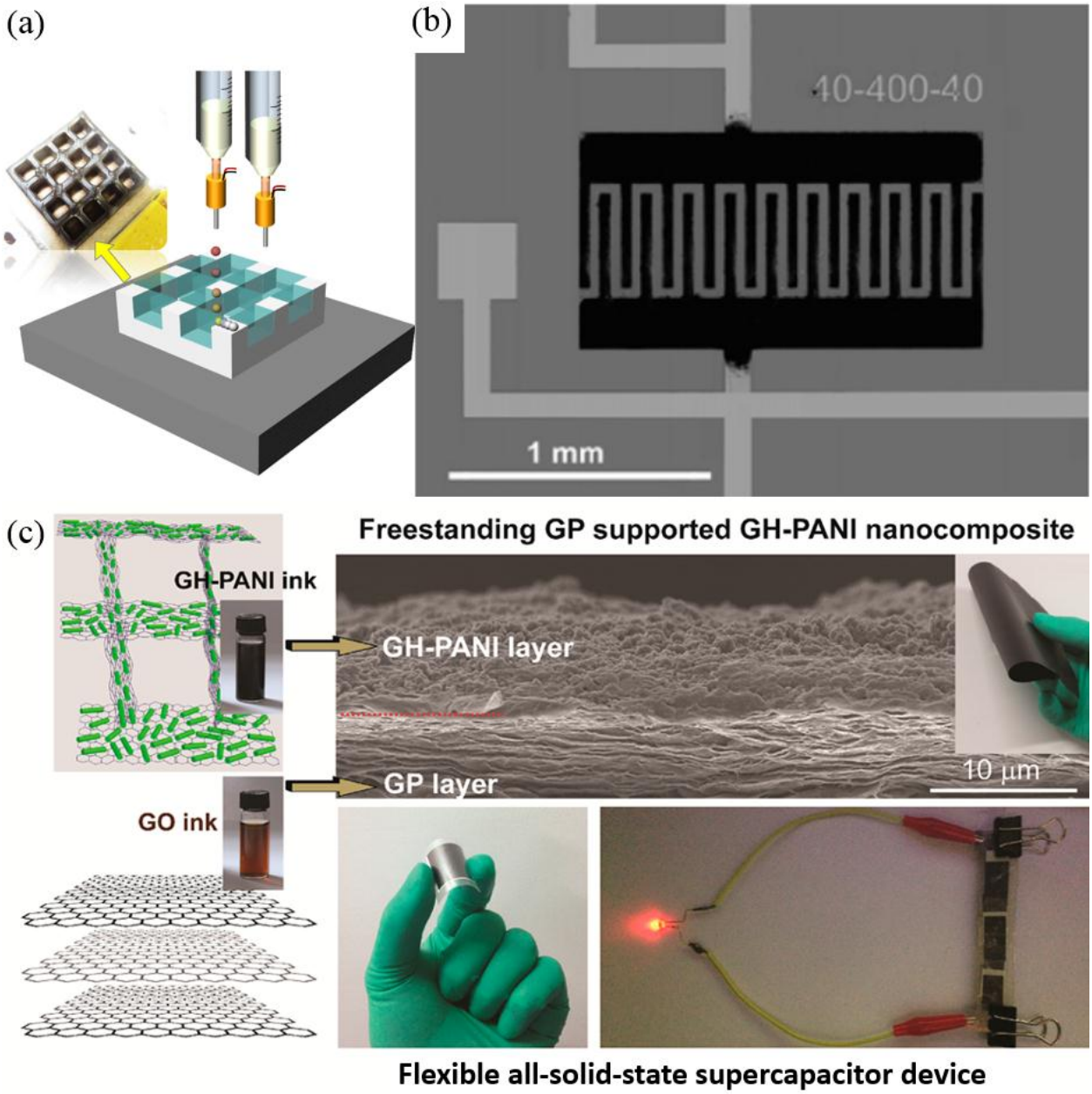

Figure 2. (a) Schematic illustration of an inkjet printing process with freezing solidification. (b) Optical image of a micro-supercapacitor with 20 fingers, 40 μm wide, 400 μm long and interspaced by 40 μm using inkjet printing technology. Reproduced with permission from [70]. (c) Schematic Illustration of the Fabrication Process of GH−PANI/GP. Multi-step inkjet printing processes are involved, including GO and GH-PANI ink seperately. Reproduced with permission from [59].

Table 1. Various inkjet printing ink prescriptions and the printer used.

Ref	Ink type	Active material	Additives (includes solvent)	3D Printer	
[71]	Conductive patterns	200 mg MWCNT, 160 mg Ag	200 mg SDBS,40 ml distilled water	HP Deskjet 1010 inkjet printer	Supercapacitor
	Anode	MnO_2, 200 mg MWCNT, 160 mg Ag,	200 mg SDBS,40 ml DI water	HP Deskjet 1010 inkjet printer	
[67]	Electrode	2mg/ml GO		DMP 2800, Dimatix	
[63]	Electrode	2mg/ml GO		DMP 2800, Dimatix	
[66]	Electrode	GO		sciFLEXARRAYER DW, Scienion, Germany	
[69]	Current collector	Silver ink		DMP 3000, Dimatix	
	Positive electrode	0.5 g/L $K_2Co_3(P_2O_7)_2{\cdot}2H_2O$ nanocrystal whiskers	Dispersant: ethanol	DMP 3000, Dimatix	
	Negative electrode	2.25 g/L graphene nanosheets	Dispersant: ethanol	DMP 3000, Dimatix	
[58]	Semi-finished electrode	0.2 mg/ml SWNTs with moderate lengths (0.5–1.5 μm)	1 wt.% aqueous SDS in DI water	Epson Artisan 50 piezoelectric printer	
[70]	Electrode	AC	5wt.% PTFE, ethylene glycol solvent, Triton X100	AltaDrop® equipment from Altatech	
[73]	Electrode	NGP powder (200 mg), PANI (200 mg)	SDBS (200 mg) and H_2O (100 mL)	Single piezoelectric nozzle	
[31]	Electrode	AC powders (50 nm), SWNTs	1.0 wt.% SDBS	HP Deskjet 1010	
	Current collector	Ag Nanowire	Water/IPA, 1/1 (v/v)	HP Deskjet 1010	
	Substrate	CNF suspension 0.1–1.0 mg/mL		HP Deskjet 1010	
	Electrolyte	IL: ([BMIM][BF_4])	ETPTA (1.0 wt.% HMPP as photoinitiator), ethanol or water as solvent	HP Deskjet 1010	
[60]	Electrode	AC	EG, Triton X100, PTFE	----	
[59]	Electrode	GO 10 mg/mL		DMP 2800, Dimatix	
	Electrode	GH−PANI nanocomposite	Water and ethanol 1:1	DMP 2800, Dimatix	
[62]	Electrolyte	PYR13-Li-TFSI		DMP 2800, Dimatix	LIB

[74]	Anode	SnO_2	AB, Hyperdispersant (CH10B, CH10B), distilled water/absolute ethanol/diethylene glycol/triethanolamine/IPA in 56:18:5:1:1	Canon BJC-1000sp printer	
[65]	Cathode	$LiCoO_2$	Surfactant-Lomar D, carbon black, PH adjust-monoethanolamine, binder-CMC sodium	Canon BJC-1000sp printer	
[61]	Cathode	carbon black, LFP	CMC, Triton X-100	Piezoelectric ink-jet printer	
[92]	Cathode	LFP coated with 2% carbon		Aerosol deposition apparatus	
[93]	Electrolyte	$Li_{1.3}Al_{0.3}Ti_{1.7}(PO4)_3$		Aerosol deposition apparatus	
[68]	Cathode	Sulfur infused SWNT-MET	CHP	DMP 2800, Dimatix	Li-Sulfur batteries
[72]	Electrode	75 wt.% MnO_2	25 wt.% PVDF-HFP, THF, 2M NH_4Cl	Lexmark 3200	Manganese
[64]	Electrode	Silver nanopaste	n-tetradecane	Customized super ink jet printing	zinc–silver
[90]	Dielectrics	(PAA) solution	aromatic hydrocarbon, NMP	DMP 2830, Dimatix	

Multiwall carbon nanotubes (MWCNT); graphene oxide (GO); polyaniline (PANI); Deionized water (DI water); sodium dodecyl sulfate (SDS); isopropylalcohol (IPA); ionic liquid (IL); polytetrafluoroethylene (PTFE); carboxymethyl cellulose (CMC); tetrahydrofuran (THF); ethylene glycol (EG); acetylene black (AB); carbon black (CB); activated carbon (AC); $LiFePO_4$ (LFP) ; $Li_4Ti_5O_{12}$ (LTO); cumene hydroperoxide (CHP); poly(amic) acid (PAA) .

2.2 Direct Ink Writing (DIW)

DIW is another 3D printing technique that utilizes direct material deposition. It is based on the extrusion of a paste-like ink with shear thinning behavior. The inks must exhibit a sufficiently high yield stress and storage modulus to allow for shape retention of the extruded lines as well as distortion-free bridging of spanning filaments. This process allows for the computer-aided build-up of consecutive layers typically into a pile-like structure. Due to the versatility and high loading of material, direct writing has been employed to fabricate batteries [51-53, 55, 94] and

supercapacitors [48, 49, 56] as a favorable 3D printing approach. The process is much less challenging compared to inkjet printing since the paste-like material is extruded and the risk of nozzle clogging is much lower than inkjet printing. In addition, very high mass loading of active materials can be used which can significantly promote the areal capacitance and energy density. However, the sophisticated manipulation to achieve high viscosity ink with shear thinning behavior is also nontrivial. **Table 2** shows various types of ink prescribed for direct writing and the related writing devices.

2.2.1 Direct ink writing of supercapacitor

Similar to inkjet printing, hydrophilic GO is also favorable in the direct ink writing of supercapacitors. Compared to the GO suspension used in inkjet printing, the GO ink used for direct writing can have very high concentration. After showing their capability to print graphene aerogel using direct-ink writing technique, Zhu *et al.* further reported the utilization of this technology in supercapacitor application [33, 95]. The electrode was composed of 3D-printed graphene composite aerogels, which was derived from supercritical drying of the as-printed 3D hierarchical structure. The GO-GNP ink used for the printing was synthesized by mixing GO suspension with graphene nanoplatelets. The self-supporting electrodes tested with the 3M KOH aqueous electrolytes can reach a specific capacitance of 63.6 F/g at a current density of 10 A/g. The quasi-solid-state, symmetric supercapacitor fabricated using two electrodes with lithium hydroxide (LiOH)/polyvinyl alcohol (PVA) gel electrolyte exhibited a maximum gravimetric capacitance of 4.76 F/g at a current density of 0.4 A/g. In addition, due to the hierarchical porous structure realized by 3D printing and supercritical drying, the rate capability of the printed three-dimensional hierarchical graphene aerogel supercapacitor electrode is among the highest compared to other reported carbon-based electrodes. The electrode fabrication process and ink

rheology are shown in **Figure 3b**. In another work**,** DIW of pristine graphene based supercapacitor electrode using special solvents was demonstrated [57]. Instead of using aqueous feedstock, the research used room temperature volatile camphene as the solvent. This strategy allows porous electrode structure to be formed under room temperature. The electrode materials used contains pristine graphene flake (PG) mixed with multiwall carbon nanotube (MWCNT), and rGO mixed with MWCNT. The addition of MWCNT, greatly increases the mechanical strength of formed aerogel, as well as effectively eliminated the restacking and aggregating of PG and rGO.

Direct ink writing has been shown to be one of the most promising 3D printing techniques for EES devices. It allows high material loading to be patterned in a controlled thickness. Yet, more materials are to be developed for supercapacitor applications.

2.2.2 Direct ink writing of batteries

Recently, Kun *et al.* printed a 3D interdigitated microbattery architecture (3D-IMA) using $Li_4Ti_5O_{12}$ (LTO) as the anode material and $LiFePO_4$ (LFP) as the cathode material [54]. LTO and LFP inks were well designed by adding deionized water, ethylene glycol, glycerol and cellulose-based viscofiers. Prior to printing, interdigitated Au current collector patterns were prepared by a combination of lithographic patterning and e-beam deposition. The LTO and LFP inks were then deposited onto a pattern to form multilayer electrodes respectively. After the printing was finished and the electrodes were dried, the LTO and LFP interdigital structure were heated to 600°C in inert gas to remove the organic additives to advance the nanoparticle sintering. Finally the 3D-IMA was packaged in a small plastic case with liquid electrolyte entrapped inside. The packaged micro-battery showed a capacity of 1.2 mAh/cm^2 at a rate of 0.5 C, and exhibited a high areal energy density of 9.7 J/cm^2 at a power density of 2.7 mW/cm^2. The areal energy and

power density of the 3D micro battery is much higher than its rechargeable counterparts due to the direct writing technology used, which enables the capability to fabricate high aspect structures within a small areal footprint. The schematic illustration of this innovative work is shown in **Figure 3a**. The bottom pane of the figure shows the paste-like ink and their rheological properties. With the same concept of direct-ink writing LIB, all component 3D-printed LIB was also presented using GO as electrode material and solid-state electrolyte inks [54]. LFP and LTO nanoparticles were added to highly concentrated GO ink to prepare the cathode and anode inks, respectively. After freeze drying and thermal reduction, the channels between the two interdigitated electrodes were filled with a polymer composite ink, which served as a separator as well as the gel polymer electrolyte. The introduction of rGO in the electrode material could greatly improve the electrical conductivity of the electrode and promote better battery electrochemical performance. In addition, only water is used as solvent for the ink. This effectively removes the necessity of high temperature burning out of organic additives as needed in previous work. More recently, carbon coated $LiMn_{0.21}Fe_{0.79}PO_4$ (LMFP) nanocrystal was used to print cathodes using DIW reaching both high rate capability and high capacity [50]. Due to the higher working voltage than that of pure LFP, a higher energy density can be achieved. With the convenient control of layer thickness achieved by DIW, the relationship between the electrode material layer thickness and the relative rate performance was investigated.

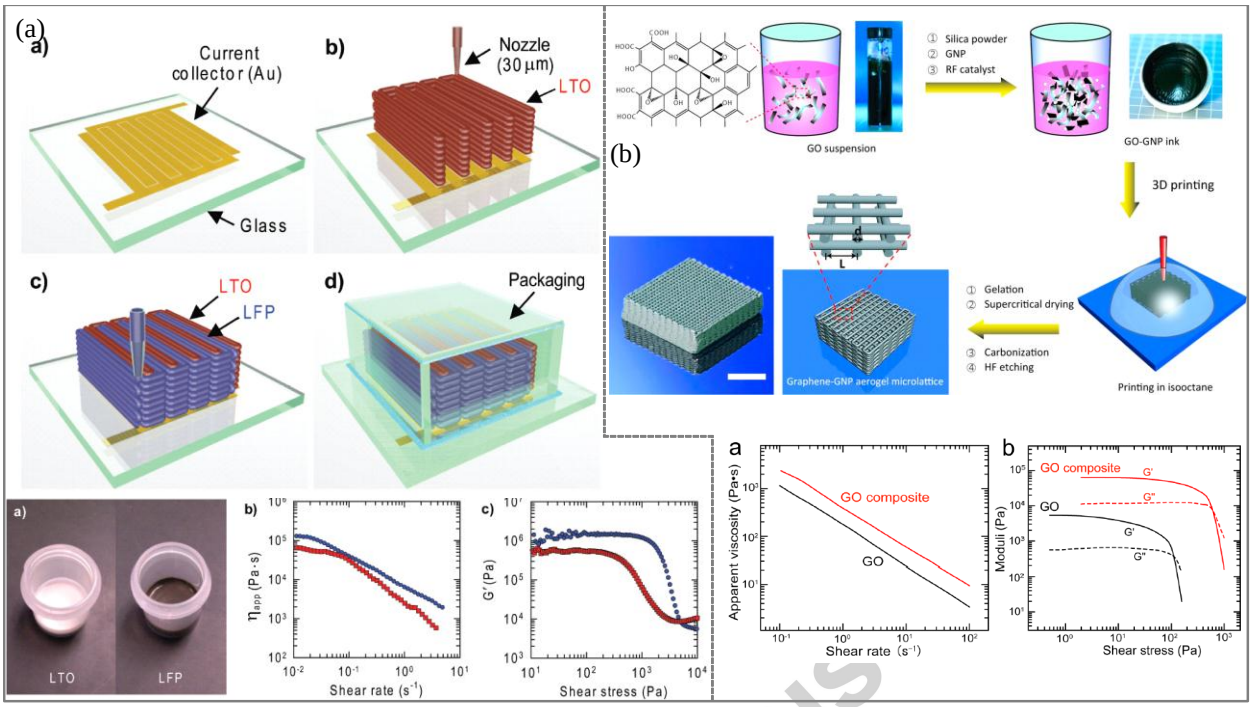

Figure 3. (a) Schematic illustration of a 3D interdigitated micro-battery architectures (3D-IMA) fabricated on a gold current collector by printing $Li_4Ti_5O_{12}$ (LTO) and $LiFePO_4$ (LFP) inks through 30 μ m nozzles, followed by sintering and packaging. Reproduced with permission from [32] (b) Supercapacitors based on 3D hierarchical graphene aerogels with periodic macropores. Reproduced with permission from [33].

Table 2. Various direct writing ink prescriptions and the printer used.

Ref	Ink type	Active material	Additives (includes solvent)	3D Printer	
[32]	Anode	55 – 65 wt.% LTO	27 wt.% Glycerol, 20 ~ 30 wt.% EG, 9 wt.% HPC, 1 wt.% HEC, and DI water	ABL 900010, Aerotech Inc.	LIB
	Cathode	55 – 65 wt.% LFP	20 wt.% glycerol, 20 ~ 30 wt.% EG, 8 wt.% HPC, 2 wt.% HEC, and DI water	ABL 900010, Aerotech Inc.	
[54]	Anode	LTO: GO 7:3		Fisnar F4200n	
	Cathode	LFP: GO 7:3		Fisnar F4200n	
	Polymer ink for electrolyte	PVDF-co-HFP : Al_2O_3 1:10	NMP	Fisnar F4200n	

[51]	Cathode	80 wt.% LTO	10 wt.% AB, 10 wt.% PVDF, 50 wt.% NMP	Self-built 3D micro patterning	
[50]	Cathode	$LiMn_{0.21}Fe_{0.79}PO_4$ (LMFP)	XC-72 CB, PVDF	self-built based on movable stage	
[94]	Cathode	80 wt.% LFP	10 wt.% CB, 10 wt.% PVDF, NMP	Self-built robot system	
	Anode	80 wt.% graphite	10 wt.% CB, 10 wt.% PVDF, NMP	Self-built robot system	
[55]	Cathode	85.5 wt.% LMO powder (13 μm)	6.5 wt.% CB ,8 wt.% PVDF, NMP	Self-built Extrusion Freeform Fabrication (EFF) system	
[53]	Current collector-Zn Air	methylcellulose with Ag powder 1:1		Self-built gantry robot	**Zn Air**
	Anode-Zn Air	65% Zn and 35% 8M KOH		Self-built gantry robot	
	Separator-Zn Air	Rescor insulating foam	Un-reported surfactant	Self-built gantry robot	
	Catalyst	50% MnO_2, 44% 8M KOH, and 6 % CB		Self-built gantry robot	
[52]	Zn electrode	95 wt.% zinc powder	5 wt.% PVDF-HFP	Self-built "drop-based" printing system	**Zn Battery**
	MnO_2 electrode	90 wt.% activated MnO_2 powder	6 wt.% AB conductive filler, 4 wt.% PVDF-HFP	Self-built "drop-based" printing system	
	Electrolyte	1:1 mixture of PVDF-HFP, 0.5 M $Zn^{+}Tf^{-}$ salt dissolved in $BMIM^{+}Tf^{-}$ IL		Self-built "drop-based" printing system	
[57]	Electrode	100 mg of graphene	5 mL phenol or camphene	Fisnar I&J7300-LF	**Supercapacitors**
[33]	Electrode	3.6 g 40 mg/cm^3 GO suspensions	2 g R-F solution, 0.3 g GNP, and 0.9 g fumed silica	ABL 9000, Aerotech	
[48]	Electrode	Highly Concentrated TRGO (thermally reduced GO)	isopropanol (15 g /L)	3D Bioplotter (Envisiontec)	
	Electrode	80% of AC	10% of additive carbon,10% CMC, IPA and distilled water	3D Bioplotter (Envisiontec)	
[56]	Electrode	20 mg/ml GO		Self-built 3D micro-extrusion system	
[49]	Electrode	6, 7, and 8wt.% CNTs	IPA, 30 wt. % dispersion agent, and EG	Self-built 3-axis positioning stage	

Graphene nanoplatelets (GNP); hydroxypropyl cellulose (HPC); hydroxyethyl cellulose (HEC); Polyvinylidene fluoride (PVDF); hexafluoropropylene (HFP); resorcinol−formaldehyde (R-F).
For other abbreviations please refer to table 1.

2.3 Freeze Nano Printing (FNP)

Recently, IJP and DIW techniques have been combined with conventional freeze casting process to define complex shaped graphene aerogels (GA) [95-97]. Our group reported the first inkjet-printed GA by directly printing aqueous GO inks onto a freezing substrate [96]. Herein we name this technology as Freeze Nano Printing (FNP). Hierarchical pore structures balancing mass transport, ion diffusion, and the diffusion length, could enable higher capacities and rate capability [91]. The importance of specific pore size to match particular ion size has been demonstrated by Chmiola *et al.* [98-100]. Aerogel is a synthetic porous material derived from a gel in which the liquid component was substituted by a gas phase. Aerogel can be facilely prepared by freeze casting (also known as ice templating) technique. The pore size and pore distributions can be tuned by using different freezing conditions, ink or slurry of different concentrations, or even by adding different additives [101-103]. GA, constructed from well-interconnected graphene sheets through freeze drying or supercritical drying, offers an innovative approach to fabricate 3D, porous graphene monolith that can work as an electrode [104].

FNP process provides great potential to achieve both high specific energy because of the increased material loading with high specific surface area and high specific power due to the hierarchical porous structure. In this process, the GO droplets of various concentrations were frozen immediately upon landing on the chilling substrate which is as low as -25 °C. The pure aqueous ink used for inkjet printing removes the necessity of undesirable fillers as only water was used as the dispersant for GO. The ingenious integrating of inkjet based freeze printing with

freeze casting technology enable the very comfortable realization of 3D complex-shape aerogels. **Figure 4** demonstrates the process of inkjet based freeze printing of 3D GA. It is worthwhile to mention that, as inkjet technology is used, concentration of GO ink as low as 0.5 mg/ml can be utilized to print GO ice structure. The successful freeze drying of such low concentration GO structure and postprocess reduction of GO enable it to be identified by the Guinness World Records as the "least dense 3D-printed structure" yet made [105].

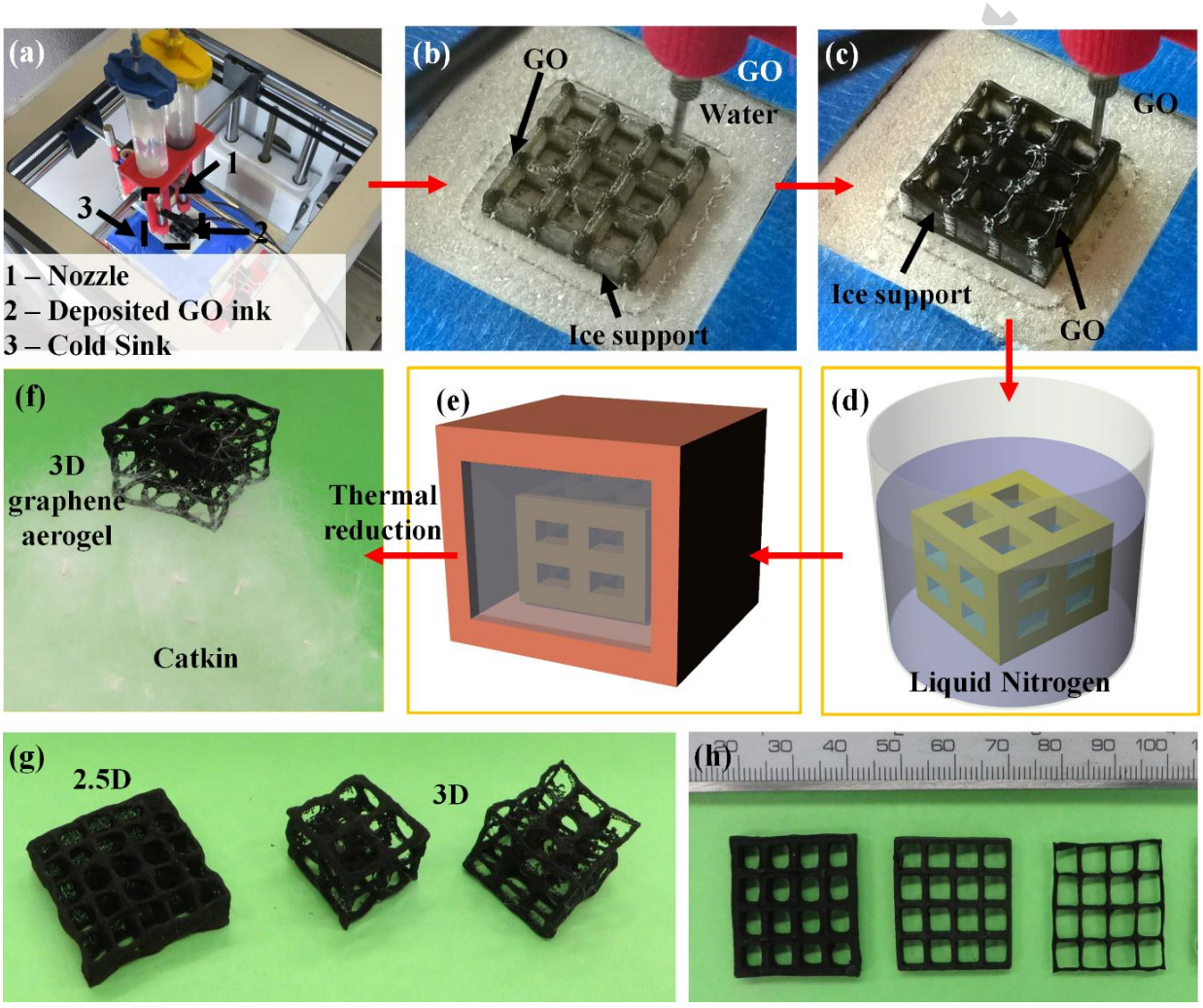

Figure 4. 3D printing of graphene aerogel (GA). (a) 3D printing setup. (b) 3D printing of ice support. (c) 3D printing of GO suspension. (d) Immersing printed ice structure into liquid nitrogen. (e) Freeze drying. (f) Thermally reduced to 3D ultra-light GA on catkin. (g) 3D GA

architecture, left: 2.5D structure and right: 3D architecture with overhang structures. (h) GAs with various wall thicknesses. Reproduced with permission from [96].

Even though combining DIW or IJP with freeze casting offers great promise to produce hierarchical porous structure that could achieve high performance, the material loading and freezing condition should be optimized to increase the accessibility of micropores to the ions. It is well worth noting that the capacitance of a material is not necessarily proportional to its SSA. Pore size distribution can also affect the performance. It tends to support that only micropores in nanometer scale are favorable for ions to enhance the capacitance. This is very challenging if not impossible for most inkjet printing devices. It can be addressed by adjusting the freeze casting parameters, such as using extreme freezing conditions and cyroprotective additives to remove the growth of large ice crystals.

2.4 Stereolithography (SLA)

SLA is a 3D printing process based on solidifying photocurable resin using light. Original SLA process utilizes a fine laser spot through a focused beam or lamp to scan over the photo curable resin, which induces a photo-polymerization and accordingly, solidification. By improving the focus of the laser spot, very fine structures can be produced by utilizing the SLA technique. Variants of the traditional SLA process include mask projection SLA (MPSL) and two-photon SLA. For the latter process, very fine features can be achieved (1 μm or less). However, the building speed of two-photon and laser scan based SLA is relatively low due to the line wise scanning. MPSL can be much faster by curing a layer in one exposure. **Figure 5**a and **Figure 5**b show a bottom-up MPSL process and an original laser scanning SLA process respectively. The materials used in the SLA process are photocurable polymers. The main ingredients in photopolymers are photoinitiators and liquid monomers. Upon shinning the resin

with light (UV or visible), the photoinitiators undergo a chemical transformation and become "reactive" with the liquid monomers to start a polymer chain, which is usually called "curing". Most of the commercially available photopolymers are developed for prototyping use, thus, are not equipped for functionality. Nevertheless, by engineering the photopolymer with other functional material such as GO [106], ceramics [107], new potential in functional usage would be possible.

Recently, a number of printed polymer/ceramic dielectric capacitors were shown by integrating stereolithography 3D printing technique with a conventional tape casting ceramic fabrication approach [81]. To prepare the ink, commercial photocurable resin Flex was mixed with silver decorated $Pb(Zr,Ti)O_3$ (PZT) nanoparticles, which was denoted as PZT@Ag (**Figure 5**c right pane shows the TEM image). The Ag could enhance the dielectric permittivity. Au electrodes were sputtered on both sides of different types of 3D printed Flex/PZT@Ag parts to act as the top and bottom electrodes respectively. The 3D printed capacitor showed a capacitance of about 63 F/g at the current density of 0.5 A/g. **Figure 5**c shows various capacitors printed by the hybrid process and their corresponding specific capacitance. This work provides an approach to fabricate the ceramic based dielectric layer in common dielectric capacitors. However, as the PZT ceramic occupies only a small portion of the composite material, and this work does not report a sintering process, it remains unclear how the photopolymer would affect the performance of the capacitors. Inspired from photolithography, Ning *et al.* demonstrated a holographic fabricated, high energy density (6.5 μWh $cm^{-2} \cdot \mu m^{-1}$), 3D mesostructured lithium-ion microbatteries based on $LiMnO_2$ cathodes, and NiSn anodes that possess supercapacitor-like power (3,600 μW $cm^{-2} \cdot \mu m^{-1}$ peak) [76]. Different from conventional photolithography,

deterministic control of both the internal electrode mesostructure and the spatial distribution of the electrodes on the substrate can be achieved using holographic.

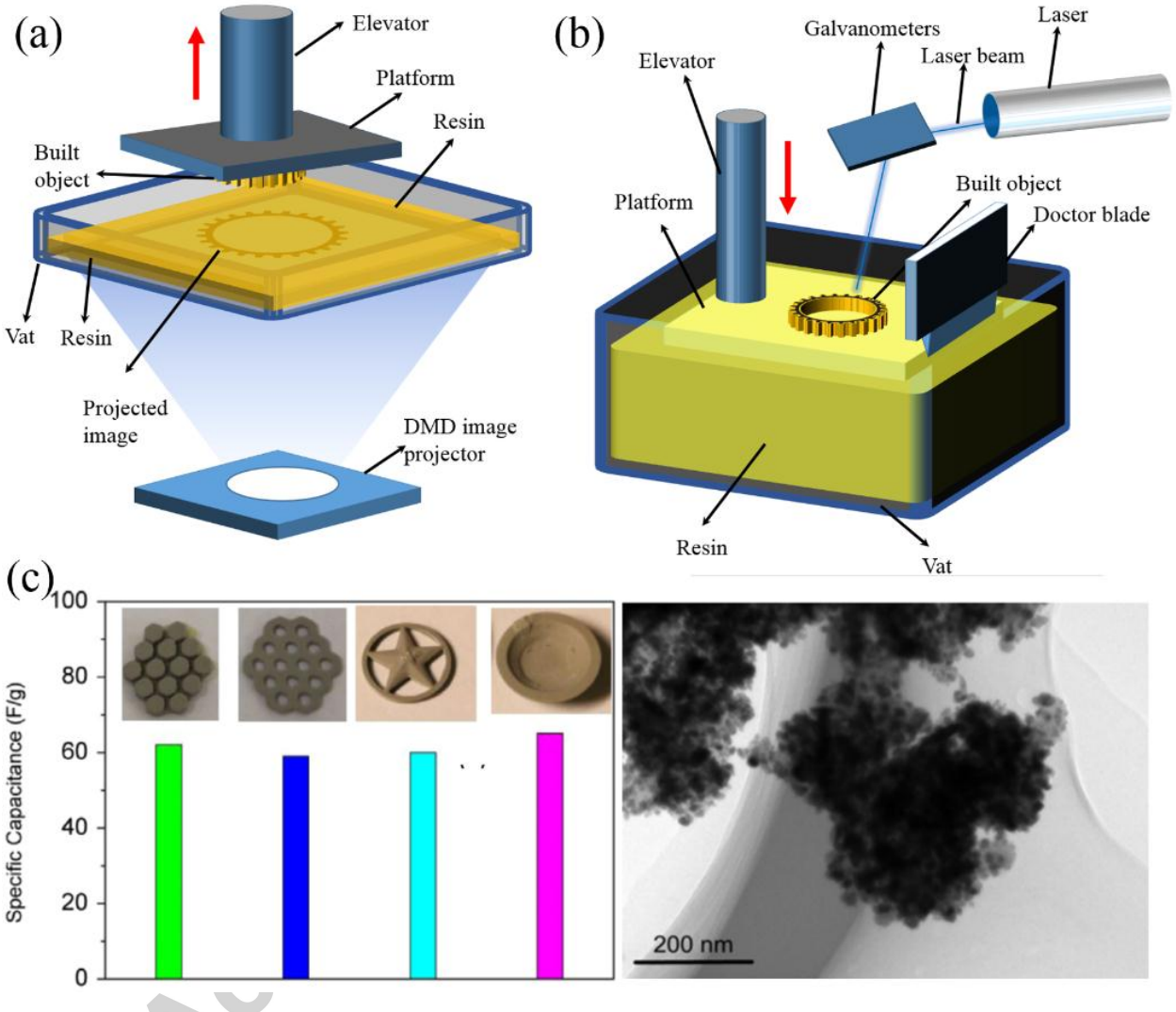

Figure 5. (a) Scheme of bottom-up mask projection stereolithography (MPSL). (b) Scheme of the traditional laser-based stereolithography (SLA). (c) Different types of dielectric capacitors realized by combining MPSL 3D printing process with tape casting. The right pane is a TEM image of the ink. Reproduced with permission from [81].

Compared to traditional EES fabrication methods, SLA can be readily used to replace photolithography based processes as photoresists in traditional photolithography are essentially

one-layer SL. Conventionally, photolithography techniques are used to pattern interdigital current collectors in traditional processes where to pattern a finger-like interdigitated electrode structure needs great effort [108, 109]. Particularly, photolithography is developed to a technique called carbon micro-electromechanical system(C-MEMS), in which patterned photoresist is pyrolyzed in an inert environment at high temperature [110]. The porosity of the pyrolyzed carbon structures can be controlled through the calcination condition or different activation methods. The C-MEMS may provide guidance for researchers to exploit SLA to print precise, truly 3-dimensional (3D) structures; and then carbonize it similarly like in C-MEMS to develop hierarchical porous 3D carbon structures which have high potential to work as electrochemical electrodes for EES devices.

2.5 Fused Deposition Modeling (FDM)

FDM is a 3D printing technique that creates 3D objects layer-by-layer by depositing filament shaped thermoplastic materials that are heated to their glass transit state. Once extruded from a brass nozzle and lands onto the substrate, the material solidifies to get a cross section of the objects created (**Figure 6**a). Common materials used in this technique are acrylonitrile–butadiene–styrene (ABS) and poly (lactic acid) (PLA) filaments. In order to use FDM printed parts as electrodes, conductive active materials must be incorporated into the ABS or PLA matrix. Both ABS and PLA have been modified to function with graphene for conductivity investigation that have potential for electrode applications [77, 78]. More recently, the composite of ABS/carbon black is also investigated [79].

The engineering of thermoplastic material with conductive fillers is nontrivial [77]. For the first step, the GO sheets and ABS were dispersed in an N-Methylpyrolidone (NMP) medium respectively. The two solutions were then mixed together and reduced by hydrazine hydrate. By

adding water and centrifuge process, the graphene-ABS composites were separated from NMP. The different states of the prescription are shown in **Figure 6b**. These graphene-polymer composites were then further thermally extruded into 1.75 mm diameter filaments to fit the commercialized 3D printer. Compared to ABS, PLA is much more environmentally friendly as it is biodegradable. The usage of PLA/graphene composite filaments to produce conductive wire shows promising result (**Figure 6c**) [78]. To fabricate the filaments, the GO was first chemically reduced by 4-iodoaniline, and then thermally reduced in a tube furnace at 1050 °C for 1 hour under the argon atmosphere. To synthesize the composite filament, the original PLA was first smashed by a pulverizer; and then homogeneously mixed with rGO by melt blending, after which graphene could be well dispersed into the PLA. Finally, the composites were processed to fabricate the composite filament with a diameter of 1.75 mm. The conductivity of the composite filaments with 6 wt. % rGO reached 476 S/m. The printed 3D structure showed excellent mechanical properties in terms of bending, stretching and bonding. However, the leading role of PLA in the composite material greatly plagued the conductivity of pure rGO, which is 60000 S/m. To overcome this problem, one strategy would be to further increase the ratio of active material through particular type of surfactant, while another approach is to remove the ABS or PLA through post-process such as calcination and etching.

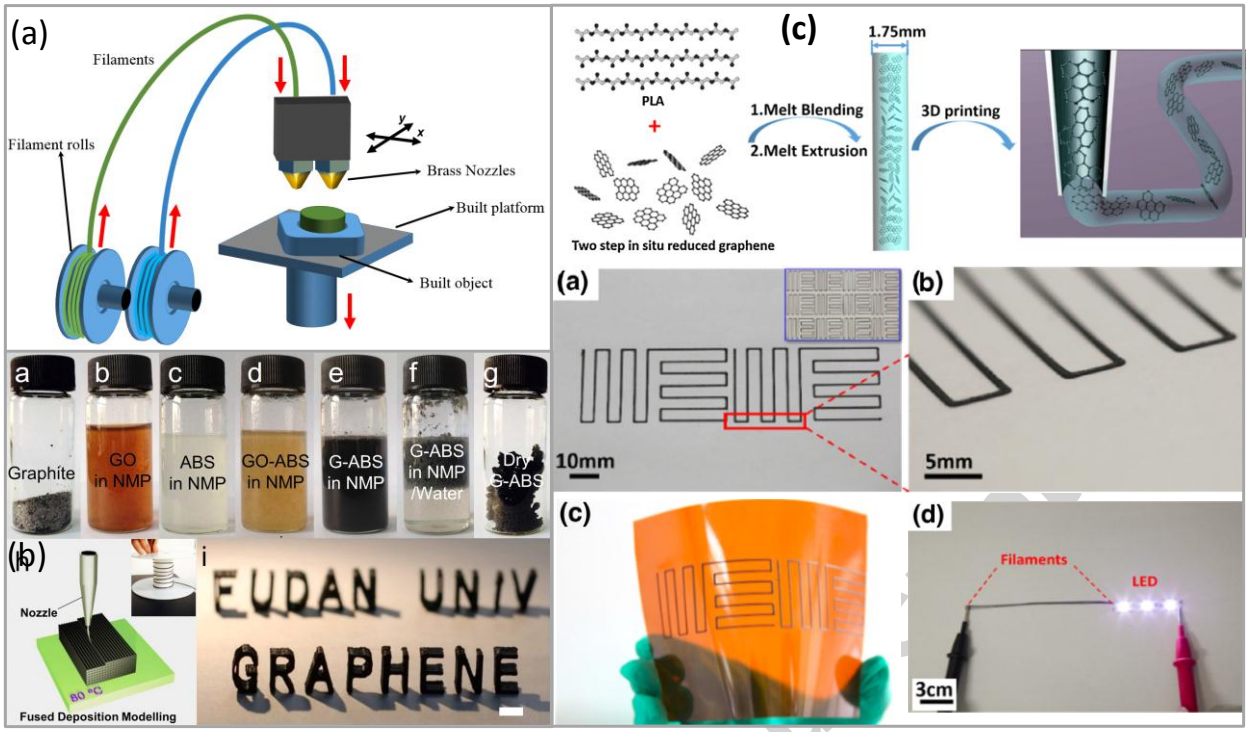

Figure 6. (a) Scheme of Fused Deposition Modeling (FDM). Thermoplastic filaments are loaded into a heated nozzle; and deposited to the platform according to pre-programmed g-code. (b) ABS-based graphene composite preparation and 3D printing using the composite filament. Reproduced with permission from [77]. (c) Scheme depicting the process of PLA-based graphene composite filament for the technique of FDM 3D printing processes. Reproduced with permission from [78].

2.6 Binder Jetting (3DP)

3DP is a powder bed based 3D printing process, wherein powder binder is inkjet deposited onto the powder bed to form a cross section of the object. Upon finishing, porous plaster-based objects can be obtained. The weak green part can be infiltrated with a second phase material to form a composite. A carbon nanofiber (CNF) impregnated plaster-based block was fabricated using 3DP printing technology [111]. To enable the infiltration of CNF, the CNF was first

dispersed in an epoxy-based infiltrant with less than 4 wt. % carbon content in the resin. A surface resistivity of below 800 Ω/sq has been acquired for the fabricated prototype. The materials of 3DP come from two portions, one is the plaster in the powder bed, while the other is the binder that is deposited onto the plaster to "glue" them together. The fabricated part from the 3DP process is normally a porous, hard solid after burning out of the binder. Because of the high porosity, it is possible to infiltrate with a second phase to form a functional composite part like what has been done in the literature above. However, the carbon content in the infiltrant is low and the conductivity of the printed part is insufficient for any practical application. 3DP may not be a good approach for applications in the EES area. Nevertheless, potential may arise, for example, by using metal oxide powders with conductive binders; an electrode may be fabricated. By using carbon-based, metal oxide powders with multiple nozzles printing of conductive and electrolyte-like binders, a promising device can be fabricated. **Figure 7** shows a 3DP process to fabricate 3D printed electrode using thermally reduced graphene oxide as powder bed [80].

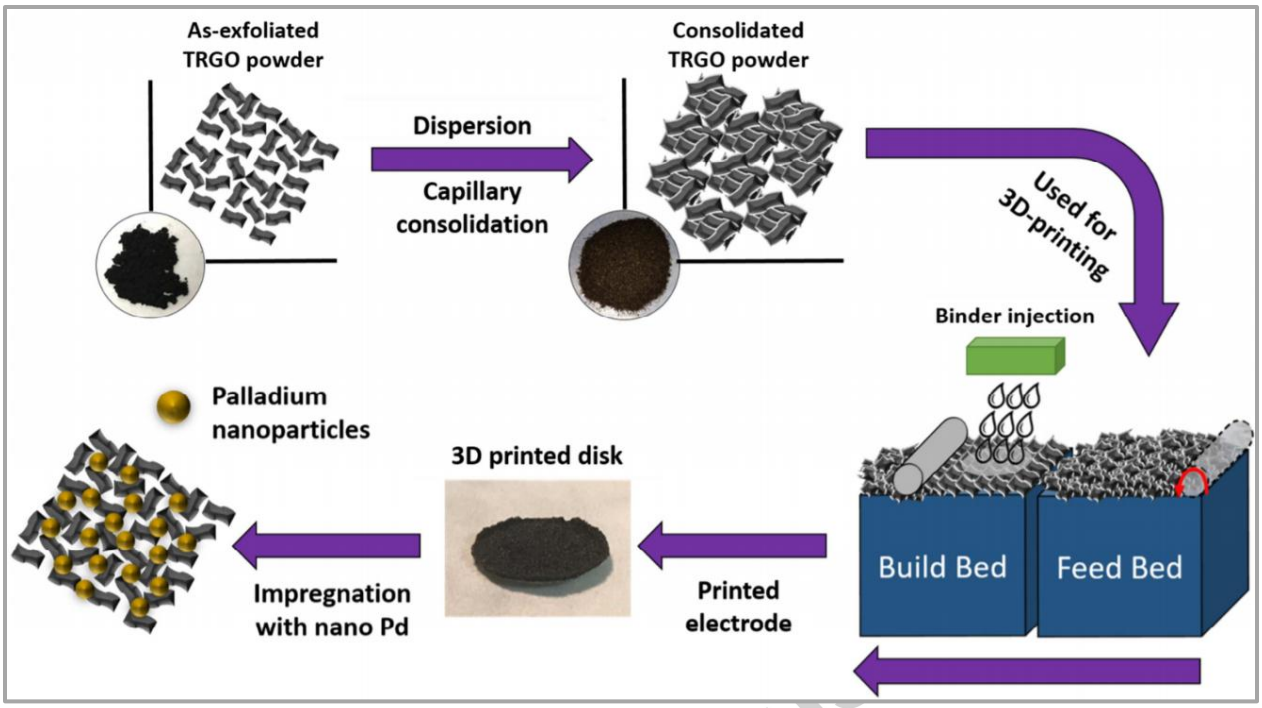

Figure 7. Scheme of presentation of the binder-jetting 3D printing process using thermally reduced graphene oxide as powder bed. Reproduced with permission from [80]

2.7 Laminated Object Manufacturing (LOM)

LOM is a 3D printing process in which layers of adhesive paper, metal, or plastic laminates are successively glued or welded together with a laminating roller. In LOM process, first a laminate of material is fed onto a stage with a material supply roll, a cross-section of the printed object is then formed with a knife or laser cutter. After the cut, sheets are recycled by a waste take-up roll. The process is repeated layer-by-layer until the entire object is created. A micro-electrode in conventional mold manufacturing was fabricated using LOM [112]. 100-μm-thick Cu foils were cut by wire-electrical discharge machining (WEDM) to obtain a cross section of the electrode 3D model. Then these 2D slices were stacked together to acquire the 3D micro-electrode through vacuum pressure thermal diffusion welding. The application of using LOM to produce an electrode for EDM can potentially guide researchers to use this technique to print the electrode

for EES devices. Furthermore, due to the material feedstock being a laminate, this 3D printing process could be potentially used to fabricate thin-film EES given the appropriate material is developed.

2.8 3D-printed metal scaffold for active material loading

Metal 3D printing is an important branch of the 3D printing technologies due to the practical implication of metal components in fields such as aerospace, automobile and biomedical areas. Metal 3D printing can mainly be categorized into one of the following four types: laser engineered net shaping (LENS), direct metal laser sintering (DMLS), selective laser melting (SLM), and electron beam melting (EBM). Among these processes, SLM is a process that uses a high-power laser beam as an energy source to create three-dimensional metal parts by fusing fine metal powders together. Very dense metal parts can be fabricated using this process. SLM technology was used to fabricate 3D titanium interdigitated electrode scaffold as shown in **Figure 8**b [84]. The as-fabricated support was electrochemically coated with PPy to form the final electrodes. Supercapacitors were assembled using the fabricated electrodes with H_3PO_4/PVA solid gel electrolyte. The as-assembled, solid-state supercapacitor with pseudocapacitive behavior achieved a volumetric capacitance of 2.4 F/cm^3 at a current density of 3.74 mA/cm^3, and a power density of 15.0 kW/m^3 at 37.4 mA/cm^3. This result is comparable to the 3D electrodes fabricated by traditional lithography processes. Due to the increased surface area realized by patterned micro-pillars, the areal energy density is much higher than previously reported planar electrodes of the same material.

Recently, DMLS was also used to produce metal scaffolds with controllable porosity which are then adapted with a co-electrodeposition of MnO_2, Mn_2O_3, and doped PEDOT:PSS as electroactive material **Figure 8**c [81]. Unlike in the SLM process where metal powder is fully

melted, DMLS process only bonds the molecules at their contact points. The printed stainless steel scaffolds consisted of a porous upper layer of 0.1mm and a fully dense supporting layer of 0.2mm. To demonstrate the effect of different current collector morphology, the performance of electrodes using different stainless steel scaffolds as current collector were compared. The electrochemical performance increased from dense plates to porous plates and porous plate to porous plate-array scaffolds. This means 3D-printed structural energy devices are of great benefit to the performance due to the higher surface area. In addition, by limiting the effects of the volumetric expansion experienced by the pseudocapacitive material using metal printed porous scaffolds of high mechanical strength, this approach offers great opportunities for hierarchical energy storage devices with improved electrochemical performance and better lifetime characteristics.

In short, metal 3D printing provides a facile way to fabricate conductive 3D support that can anchor thin layer of pseudo-capacitive materials. These artificial 3D structures not only create paths for electrolyte penetration, but also serve as current collectors that facilitate the transport of electrons. **Figure 8**a clearly shows this intent.

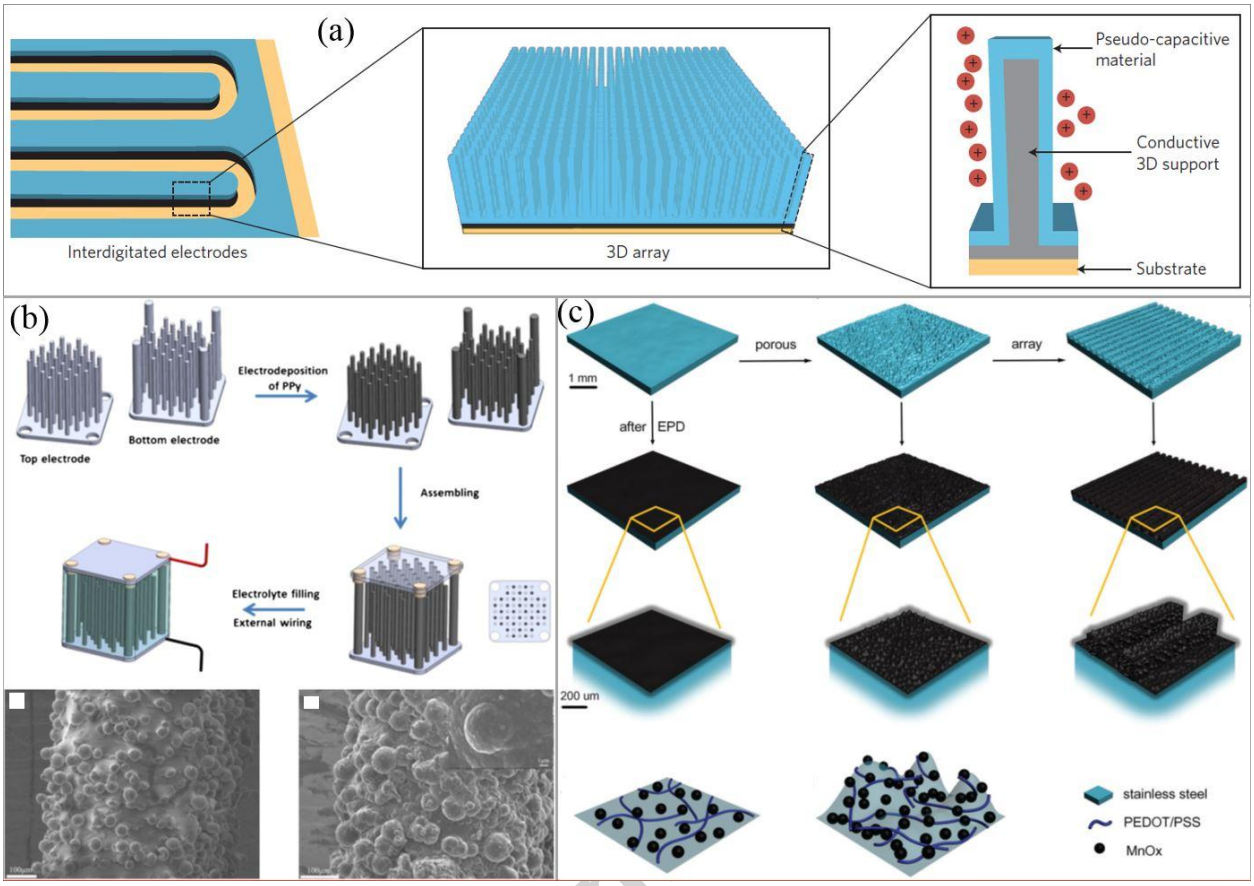

Figure 8. (a) Schematic representation of an interdigitated microsupercapacitor with an internal 3D architecture. Reproduced with permission from [113]. (b) Schematic procedures used to fabricate solid-state supercapacitors, including interdigitated Ti electrode design, PPy electropolymerization and device assembly. Reproduced with permission from [84]. (c) Scheme of 3D-printed stainless steel scaffolds and electrodeposited MnO_x-PEDOT: PSS. 3D-printed stainless steel scaffolds of three types: standard dense plate, porous plate, and porous plate and array. Reproduced with permission from [81].

3. Material requirements for 3D printing of EES

Most of the supercapacitors and batteries are composed of four components: electrode (anode and cathode), electrolyte, separator and current collector. The processing of electrolyte and

current collector is relatively less complicated compared to electrode in conventional methods. However, the assembly of electrolytes and current collectors to form final device are also important, and the processes are much different in 3D printing scenario.

3.1 Electrolyte considerations

The electrolyte serves as a medium for ion storage, transport, and electrodes separation. Among different electrolyte materials, gel electrolytes have attracted increasing attention for use in solid-state supercapacitors. Conventionally, the electrolyte is assembled into the device via approaches of dip-coating, drop-casting, or injection. The process is usually finished at the last step of device fabrication and isolated from electrode fabrication, which greatly limits the efficiency for large-scale manufacturing. Due to the state of most electrolytes being either liquid or colloid gel, it is possible to fabricate all-printed devices using inkjet printing and direct writing 3D printing techniques. However, issues may rise in some type of the electrolyte like a strong acid or strong alkaline, which may cause corrosion to the deposition nozzles. Therefore, special nozzles that are acid-resistant and alkaline-resistant should be explored further. Ionic liquids (ILs) based electrolyte would be favorable for 3D printing if all-printed device is to be considered, as ILs contribute much less corrosion to the printed device and it can work at higher voltage. The ability to work at high voltage would be beneficial to both specific energy and power densities.

3.2 Current collector considerations

Current collector is a necessary component in most of the cases where the conductivity of the electrode is insufficient to output the electronics. Therefore, the consideration of integration of current collectors into the fabrication process is an important step for all-printed devices. In the case of flexible thin film applications, the exploration of suitable current collectors which exhibit

high flexibility is desirable. However, from the perspective of fabrication, directly using immediately available current collectors will significantly decrease the fabrication costs. It would be relatively simple to use available metal foil as current collectors in sandwich-like structure. However, in the case of in-plane design especially with interdigitated structures, issues like short circuit need to be considered. Ideally, the current can be eliminated if the conductivity of electrode is sufficiently high. This could be realized by engineering active material through doping or coating with nanomaterials that possess excellent electric conductivity.

3.3 Multi-material processing

To enable the fabrication of all-3D printed energy storage devices, it is important to understand the input material requirement, the output material capability of each process, and the multi-material printing capability. A summary of this aspect regarding 3D printing processes is shown in **Table 3**.

Table 3. Material feedstock requirements of 3D printing processes.

Processes	Input material	Output material	Multi-material capability
Inkjet printing	Low viscosity Newtonian liquid	Porous solid/solid	Very good
Direct writing	High viscosity non-Newtonian paste	Varies	Good
SLA	Photosensitive resin	Mainly hard solid	Challenging
FDM	ABS or PLA Filament doped with active material	Hard solid	Possible but not applicable to EES
LOM	Paper, plastic or metal Laminates	Flexible/hard solid	Challenging
SLM	Metal powders	Hard solid	Very Challenging
3DP	Powders (ceramics, polymer, metal)	Porous hard solid	Very Challenging

4. Summary and Perspective

We have reviewed innovative 3D printing technologies for EES devices fabrication. Compared to traditional fabrication techniques, 3D printing shows several advantages in terms of performance, environmental factors, cost, and scalability. The most pronounced benefit of using 3D printing comes from its excellent patterning capability. This advantage allows 3D printing to pattern complex shaped 2D structures as well as hierarchical 3D architectures. The conveniently patterned interdigital planar structure could potentially promote the specific power density of EES because of the shortened ion transport route. The hierarchical 3D structure enables the increase of active material loading as well as facilitates fast ion transport through the porous structure realized by 3D printing, thus simultaneously leading to high specific energy and power densities. Among various 3D printing processes, direct writing and inkjet printing are extensively studied due to their similarities to conventional methods regarding material feedstock. However, both techniques require the printing ink to be well formulated. While inkjet printing requires low viscosity Newtonian liquid-like ink, direct writing needs the ink to be high viscosity, i.e. non-Newtonian paste with shear-thinning behavior. Compared to inkjet printing, direct writing can print the electrode with a much higher active material loading and with much less clogging risk. Nevertheless, inkjet printing provides much higher resolution as well as excellent multi-material deposition capability owing to the drop-on-demand nature. Among others, LOM is a roll-to-roll based process, it would be quite suitable to produce flexible device with particular shapes, which have the potential to be integrated into wearable electrical devices by stacking a few layers. FDM and SLA are the main types of desktop 3D printing techniques. SLA techniques provide the capability to print a part with high resolution, while FDM may represent the cheapest 3D printing techniques.

One of the greatest challenges in 3D printing to fabricate EES devices is the limitations in available materials that can be adapted to this new technology. Currently, the materials that have been used to produce electrodes via 3D printing are still quite limited compared to the large number of materials extensively used in conventional processes. Most of the already attempted materials in 3D printing area are not optimized yet for the process due to several practical reasons such as the lack of thorough understanding of each process and its material property requirements. Current materials are mainly developed for conventional fabrication techniques. To fit the emerging 3D printing techniques, materials that are suitable for each 3D printing process are required for the specific technology to be properly utilized. In some cases, even though 3D printed devices outperform their counterparts fabricated using traditional techniques, the ink is still not fully optimized. With the well optimized material, it is anticipated that the performance achieved by 3D printing could be further improved. Therefore, massive research effort is needed to thoroughly engineer the appropriate material that lends itself to an optimal ink formulation for 3D printing. The emerging of 3D printing as a novel approach to fabricate devices requires researchers in this area to rethink how materials should be prepared.

It is clear that fully printed batteries and supercapacitors are essential for on chip integration and industrial application of EES devices. Currently, it is still very challenging to fabricate fully 3D-printed energy devices. Most of the 3D printing processes can only fabricate one or two components of the device but not an entire device. Inkjet printing and direct writing provide the possibility to fabricate most of the key components of devices simultaneously by preparing applicable electrode ink, electrolyte ink, and even current collector ink due to the excellent multi-material printing capability of these processes. However, fabricating a fully enclosed/packaged

device is a challenge. Thus, it is a promising route to develop an integrated, hybrid printing chain to realize the process from printing material to immediately usable device.

From the perspective of design and fabrication, it would be quite promising to combine emerging 3D printing processes with conventional fabrication techniques. Since higher energy density requires thicker electrodes or higher mass per unit volume, while high rate performance prefers thin or porous electrode, a thick but porous electrode could obtain both high specific energy and power densities. For example, by integrating the capability to create flexible, complex geometry of 3D printing with large specific surface area realized by conventional freeze casting method, hierarchical porous electrode structures can be obtained. This method can potentially yield both high specific energy and specific power. Moreover, when EES geometries extend beyond simple squares or circles, the software design and simulation of the proposed structures would also become important [114, 115]. Therefore, the proper development of EES models and simulation software would promote the truly customized power device. The advanced computer aided design (CAD) integration with the 3D printing computer aided manufacturing (CAM) technology together will guide researchers to rethink the fabrication of future power sources. Overall, 3D printing, is expected to be a disruptive innovation that changes the way we think about fabricating and integrating energy storage devices [116]. The transformation of conventional EES fabrication towards new 3D printing innovative technologies will lead to the next generation of highly embedded electronics, flexible devices, and inconspicuous wearable systems.

Acknowledgments

This work is financially supported from the SUNY Network of Excellence in Materials and Advanced Manufacturing program along with the Sustainable Manufacturing and Advanced

Robotics Technology (SMART) Community of Excellence program at the University at Buffalo. V.V. and Y.S. thank the support of the Laboratory Directed Research and Development (LDRD) program at the Pacific Northwest National Laboratory (PNNL). PNNL is operated by Battelle for the DOE under Contract DE–AC05–76RLO1830.

References

[1] S. Chu, A. Majumdar, *Nature* 488 (2012) 294-303.

[2] M. Winter, R. J. Brodd, *Chem. Rev.* 104 (2004) 4245-4270.

[3] J. R. Miller, P. Simon, *Science* 321 (2008) 651-652.

[4] P. Simon, Y. Gogotsi, *Nat. Mater.* 7 (2008) 845-854.

[5] B. Mendoza-Sánchez, Y. Gogotsi, *Adv. Mater.* 28 (2016) 6104-6135.

[6] X. Peng, H. Liu, Q. Yin, J. Wu, P. Chen, G. Zhang, G. Liu, C. Wu, Y. Xie, *Nat. Commun.* 7 (2016) 11782.

[7] J. H. Pikul, H. G. Zhang, J. Cho, P. V. Braun, W. P. King, *Nat. Commun.* 4 (2013) 1732.

[8] M. M. Shaijumon, E. Perre, B. Daffos, P. L. Taberna, J. M. Tarascon, P. Simon, *Adv. Mater.* 22 (2010) 4978-4981.

[9] J. W. Long, B. Dunn, D. R. Rolison, H. S. White, *Chem. Rev.* 104 (2004) 4463-4492.

[10] T. S. Arthur, D. J. Bates, N. Cirigliano, D. C. Johnson, P. Malati, J. M. Mosby, E. Perre, M. T. Rawls, A. L. Prieto, B. Dunn, *MRS Bull.* 36 (2011) 523-531.

[11] M. Beidaghi, C. Wang, *Adv. Funct. Mater.* 22 (2012) 4501-4510.

[12] J. H. Kim, K.-W. Nam, S. B. Ma, K. B. Kim, *Carbon* 44 (2006) 1963-1968.

[13] M. Beidaghi, C. Wang, *Electrochim. Acta* 56 (2011) 9508-9514.

[14] I.-H. Kim, J.-H. Kim, Y.-H. Lee, K.-B. Kim, *J. Electrochem. Soc.* 152 (2005) A2170-A2178.

[15] C. Du, N. Pan, *J. Power Sources* 160 (2006) 1487-1494.

[16] D. Pech, M. Brunet, H. Durou, P. Huang, V. Mochalin, Y. Gogotsi, P.-L. Taberna, P. Simon, *Nat. Nanotechnol.* 5 (2010) 651-654.

[17] J. Broughton, M. Brett, *Electrochim. Acta* 49 (2004) 4439-4446.

[18] Y. Yoon, W. Cho, J. Lim, D. Choi, *J. Power Sources* 101 (2001) 126-129.

[19] J. J. Yoo, K. Balakrishnan, J. Huang, V. Meunier, B. G. Sumpter, A. Srivastava, M. Conway, A. L. Mohana Reddy, J. Yu, R. Vajtai, *Nano Lett.* 11 (2011) 1423-1427.

[20] J. R. Miller, R. Outlaw, B. Holloway, *Science* 329 (2010) 1637-1639.

[21] C. Guan, J. Liu, Y. Wang, L. Mao, Z. Fan, Z. Shen, H. Zhang, J. Wang, *ACS Nano* 9 (2015) 5198-5207.

[22] H. R. Byon, S. W. Lee, S. Chen, P. T. Hammond, Y. Shao-Horn, *Carbon* 49 (2011) 457-467.

[23] X. Dong, L. Wang, D. Wang, C. Li, J. Jin, *Langmuir* 28 (2011) 293-298.

[24] S. C. Pang, M. A. Anderson, T. W. Chapman, *J. Electrochem. Soc.* 147 (2000) 444-450.

[25] R. N. Reddy, R. G. Reddy, *J. Power Sources* 124 (2003) 330-337.

[26] Z. S. Wu, K. Parvez, X. Feng, K. Müllen, *Nat. Commun.* 4 (2013) 2487.

[27] S. Vozar, Y.-C. Poh, T. Serbowicz, M. Bachner, P. Podsiadlo, M. Qin, E. Verploegen, N. Kotov, A. J. Hart, *Review of Scientific Instruments* 80 (2009)p. 023903.

[28] S. J. An, Y. Zhu, S. H. Lee, M. D. Stoller, T. Emilsson, S. Park, A. Velamakanni, J. An, R. S. Ruoff, *J. Phys. Chem. Lett.* 1 (2010) 1259-1263.

[29] Y.-M. Chiang, W. C. Carter, J. C. Cross III, R. Bazzarella, N. Ota, "Semi-solid electrode cell having a porous current collector and methods of manufacture," U.S. Patent Application No. 13/606,986.

[30] P. Yang, W. Mai, *Nano Energy* 8 (2014) 274-290.

[31] K.-H. Choi, J. Yoo, C. K. Lee, S.-Y. Lee, *Energy Environ Sci.* 9 (2016) 2812-2821.

[32] K. Sun, T. S. Wei, B. Y. Ahn, J. Y. Seo, S. J. Dillon, J. A. Lewis, *Adv. Mater.* 25 (2013) 4539-4543.

[33] C. Zhu, T. Liu, F. Qian, T. Y.-J. Han, E. B. Duoss, J. D. Kuntz, C. M. Spadaccini, M. A. Worsley, Y. Li, *Nano Lett.* 16 (2016) 3448-3456.

[34] M. Wei, F. Zhang, W. Wang, P. Alexandridis, C. Zhou, G. Wu, *Journal of Power Sources* 354 (2017) 134–147.

[35] Astm standard f2792, standard terminology for additive manufacturing technologies. 2013. URL: http://www.astm.org/Standards/F2792.htm.

[36] Y. Zheng, Z.-Z. He, J. Yang, J. Liu, *Sci. Rep.* 4 (2014)p. 4588.

[37] E. Macdonald, R. Salas, D. Espalin, M. Perez, E. Aguilera, D. Muse, R. B. Wicker, *IEEE Access* 2 (2014) 234-242.

[38] J. A. Lewis, *Adv. Funct. Mater.* 16 (2006) 2193-2204.

[39] D. T. Nguyen, C. Meyers, T. D. Yee, N. A. Dudukovic, J. F. Destino, C. Zhu, E. B. Duoss, T. F. Baumann, T. Suratwala, J. E. Smay, *Adv. Mater.* 29 (2017) 1701181.

[40] F. Kotz, K. Arnold, W. Bauer, D. Schild, N. Keller, K. Sachsenheimer, T. M. Nargang, C. Richter, D. Helmer, B. E. Rapp, *Nature* 544 (2017) 337-339.

[41] The Wall Street Journal, GE, Rivals Turn to Europe For Push Into 3-D Printing. http://www.foxbusiness.com/features/2017/05/08/ge-rivals-turn-to-europe-for-push-into-3-d-printing-wsj.html, 2017 (accessed 17.05.08).

[42] Fortune, 3D Printing Titanium Parts Could Save Boeing Millions on Dreamliner Production. http://fortune.com/2017/04/11/3d-printing-norsk-boeing-dreamliner/, 2017 (accessed 17.05.08).

[43] M. S. Mannoor, Z. Jiang, T. James, Y. L. Kong, K. A. Malatesta, W. O. Soboyejo, N. Verma, D. H. Gracias, M. C. McAlpine, *Nano Lett.* 13 (2013) 2634-2639.

[44] J. Zuniga, D. Katsavelis, J. Peck, J. Stollberg, M. Petrykowski, A. Carson, C. Fernandez, *BMC research notes* 8 (2015) 10.

[45] X. Zheng, H. Lee, T. H. Weisgraber, M. Shusteff, J. DeOtte, E. B. Duoss, J. D. Kuntz, M. M. Biener, Q. Ge, J. A. Jackson, *Science* 344 (2014) 1373-1377.

[46] T. A. Schaedler, A. J. Jacobsen, A. Torrents, A. E. Sorensen, J. Lian, J. R. Greer, L. Valdevit, W. B. Carter, *Science* 334 (2011) 962-965.

[47] D. L. Cohen, J. I. Lipton, M. Cutler, D. Coulter, A. Vesco, H. Lipson, "Hydrocolloid printing: a novel platform for customized food production," in *Solid Freeform Fabrication Symposium*, 2009, pp. 807-818.

[48] T. Nathan-Walleser, I. M. Lazar, M. Fabritius, F. J. Tölle, Q. Xia, B. Bruchmann, S. S. Venkataraman, M. G. Schwab, R. Mülhaupt, *Adv. Funct. Mater.* 24 (2014) 4706-4716.

[49] W. Yu, H. Zhou, B. Q. Li, S. Ding, *ACS Appl. Mater. Interfaces* 9 (2017) 4597-4604.

[50] J. Hu, Y. Jiang, S. Cui, Y. Duan, T. Liu, H. Guo, L. Lin, Y. Lin, J. Zheng, K. Amine, *Adv. Energy Mater.* 6 (2016) 1600856.

[51] A. Izumi, M. Sanada, K. Furuichi, K. Teraki, T. Matsuda, K. Hiramatsu, H. Munakata, K. Kanamura, *Electrochim. Acta* 79 (2012) 218-222.

[52] C. C. Ho, J. W. Evans, P. K. Wright, *J. Micromech. Microeng.* 20 (2010) 104009.

[53] E. Malone, K. Rasa, D. Cohen, T. Isaacson, H. Lashley, H. Lipson, *RAPID PROTOTYPING J* 10 (2004) 58-69.

[54] K. Fu, Y. Wang, C. Yan, Y. Yao, Y. Chen, J. Dai, S. Lacey, Y. Wang, J. Wan, T. Li, *Adv. Mater.* 28 (2016) 2587-2594.

[55] J. Li, M. C. Leu, R. Panat, J. Park, *Mater. Des.* 119 (2017) 417-424.

[56] G. Sun, J. An, C. K. Chua, H. Pang, J. Zhang, P. Chen, *Electrochem. Commun.* 51 (2015) 33-36.

[57] Y. Lin, F. Liu, G. Casano, R. Bhavsar, I. A. Kinloch, B. Derby, *Adv. Mater.* 28 (2016) 7993-8000.

[58] P. Chen, H. Chen, J. Qiu, C. Zhou, *Nano Res.* 3 (2010) 594-603.

[59] K. Chi, Z. Zhang, J. Xi, Y. Huang, F. Xiao, S. Wang, Y. Liu, *ACS Appl. Mater. Interfaces* 6 (2014) 16312-16319.

[60] V. Conédéra, F. Mesnilgrente, M. Brunet, N. Fabre, "Fabrication of activated carbon electrodes by inkjet deposition," in *Quantum, Nano and Micro Technologies, 2009. ICQNM'09. Third International Conference on*, 2009, pp. 157-161.

[61] P.-E. Delannoy, B. Riou, T. Brousse, J. Le Bideau, D. Guyomard, B. Lestriez, *J. Power Sources* 287 (2015) 261-268.

[62] P.-E. Delannoy, B. Riou, B. Lestriez, D. Guyomard, T. Brousse, J. Le Bideau, *J. Power Sources* 274 (2015) 1085-1090.

[63] M. H. Ervin, L. T. Le, W. Y. Lee, *Electrochim. Acta* 147 (2014) 610-616.

[64] C. C. Ho, K. Murata, D. A. Steingart, J. W. Evans, P. K. Wright, *J. Micromech. Microeng.* 19 (2009) 094013.

[65] J. Huang, J. Yang, W. Li, W. Cai, Z. Jiang, *Thin Solid Films* 516 (2008) 3314-3319.

[66] H. Jung, C. V. Cheah, N. Jeong, J. Lee, *Appl. Phys. Lett.* 105 (2014) 053902.

[67] L. T. Le, M. H. Ervin, H. Qiu, B. E. Fuchs, W. Y. Lee, *Electrochem. Commun.* 13 (2011) 355-358.

[68] C. A. Milroy, S. Jang, T. Fujimori, A. Dodabalapur, A. Manthiram, *Small* 13 (2017) 1603786.

[69] H. Pang, Y. Zhang, W.-Y. Lai, Z. Hu, W. Huang, *Nano Energy* 15 (2015) 303-312.

[70] D. Pech, M. Brunet, P.-L. Taberna, P. Simon, N. Fabre, F. Mesnilgrente, V. Conédéra, H. Durou, *J. Power Sources* 195 (2010) 1266-1269.

[71] S. Wang, N. Liu, J. Tao, C. Yang, W. Liu, Y. Shi, Y. Wang, J. Su, L. Li, Y. Gao, *J. Mater. Chem. A* 3 (2015) 2407-2413.

[72] F. Xu, T. Wang, W. Li, Z. Jiang, *Chem. Phys. Lett.* 375 (2003) 247-251.

[73] Y. Xu, I. Hennig, D. Freyberg, A. J. Strudwick, M. G. Schwab, T. Weitz, K. C.-P. Cha, *J. Power Sources* 248 (2014) 483-488.

[74] Y. Zhao, Q. Zhou, L. Liu, J. Xu, M. Yan, Z. Jiang, *Electrochim. Acta* 51 (2006) 2639-2645.

[75] Y. Yang, Z. Chen, X. Song, B. Zhu, T. Hsiai, P.-I. Wu, R. Xiong, J. Shi, Y. Chen, Q. Zhou, *Nano Energy* 22 (2016) 414-421.

[76] H. Ning, J. H. Pikul, R. Zhang, X. Li, S. Xu, J. Wang, J. A. Rogers, W. P. King, P. V. Braun, *Proc. Natl. Acad. Sci. U.S.A.* 112 (2015) 6573-6578.

[77] X. Wei, D. Li, W. Jiang, Z. Gu, X. Wang, Z. Zhang, Z. Sun, *Sci. Rep.* 5 (2015) 11181.

[78] D. Zhang, B. Chi, B. Li, Z. Gao, Y. Du, J. Guo, J. Wei, *Synth. Met.* 217 (2016) 79-86.

[79] J. Zhang, B. Yang, F. Fu, F. You, X. Dong, M. Dai, *Applied Sciences* 7 (2017) 20.

[80] A. Azhari, E. Marzbanrad, D. Yilman, E. Toyserkani, M. A. Pope, *Carbon* 119 (2017) 257-266.

[81] X. Liu, R. Jervis, R. C. Maher, I. J. Villar-Garcia, M. Naylor-Marlow, P. R. Shearing, M. Ouyang, L. Cohen, N. P. Brandon, B. Wu, *Advanced Materials Technologies* 1 (2016) 1600167.

[82] K. A. Ibrahim, B. Wu, N. P. Brandon, *Mater. Des.* 106 (2016) 51-59.

[83] A. Ambrosi, J. G. S. Moo, M. Pumera, *Adv. Funct. Mater.* 26 (2016) 698-703.

[84] C. Zhao, C. Wang, R. Gorkin, S. Beirne, K. Shu, G. G. Wallace, *Electrochem. Commun.* 41 (2014) 20-23.

[85] M. Singh, H. M. Haverinen, P. Dhagat, G. E. Jabbour, *Adv. Mater.* 22 (2010) 673-685.

[86] B. Derby, *Annu. Rev. Mater. Res.* 40 (2010) 395-414.

[87] L. L. Zhang, X. Zhao, *Chem. Soc. Rev.* 38 (2009) 2520-2531.

[88] D. Xiong, X. Li, H. Shan, Y. Zhao, L. Dong, H. Xu, X. Zhang, D. Li, X. Sun, *Electrochim. Acta* 174 (2015) 762-769.

[89] F. Zhang, F. Yang, D. Lin, C. Zhou, *J. Manuf. Sci. Eng.* 139 (2017) 031016.

[90] F. Zhang, C. Tuck, R. Hague, Y. He, E. Saleh, Y. Li, C. Sturgess, R. Wildman, *J. Appl. Polym. Sci.* 133 (2016). 11.

[91] W. Yuan, Y. Zhang, L. Cheng, H. Wu, L. Zheng, D. Zhao, *J. Mater. Chem. A* 4 (2016) 8932-8951.

[92] I. Kim, J. Park, T.-H. Nam, K.-W. Kim, J.-H. Ahn, D.-S. Park, C. Ahn, G. Wang, H.-J. Ahn, *J. Power Sources* 244 (2013) 646-651.

[93] D. Popovici, H. Nagai, S. Fujishima, J. Akedo, *J. Am. Ceram. Soc.* 94 (2011) 3847-3850.

[94] Y. H. Ying, "New generation 3D printed on-chip energy storage devices," in *Electron Devices and Solid-State Circuits (EDSSC), 2016 IEEE International Conference on*, 2016, pp. 472-475.

[95] C. Zhu, T. Y.-J. Han, E. B. Duoss, A. M. Golobic, J. D. Kuntz, C. M. Spadaccini, M. A. Worsley, *Nat. Commun.* 6 (2015) 6962.

[96] Q. Zhang, F. Zhang, S. P. Medarametla, H. Li, C. Zhou, D. Lin, *Small* 12 (2016) 1702–1708.

[97] E. García-Tuñon, S. Barg, J. Franco, R. Bell, S. Eslava, E. D'Elia, R. C. Maher, F. Guitian, E. Saiz, *Adv. Mater.* 27 (2015) 1688-1693.

[98] J. Chmiola, G. Yushin, Y. Gogotsi, C. Portet, P. Simon, P.-L. Taberna, *Science* 313 (2006) 1760-1763.

[99] J. Huang, B. G. Sumpter, V. Meunier, *Angew. Chem. Int. Ed.* 47 (2008) 520-524.

[100] J. Huang, B. G. Sumpter, V. Meunier, *Chem. Eur. J.* 14 (2008) 6614-6626.

[101] P. Hao, Z. Zhao, J. Tian, H. Li, Y. Sang, G. Yu, H. Cai, H. Liu, C. Wong, A. Umar, *Nanoscale* 6 (2014) 12120-12129.

[102] X. Zhang, Z. Sui, B. Xu, S. Yue, Y. Luo, W. Zhan, B. Liu, *J. Mater. Chem.* 21 (2011) 6494-6497.

[103] S. Deville, *Adv. Eng. Mater.* 10 (2008) 155-169.

[104] Z. S. Wu, A. Winter, L. Chen, Y. Sun, A. Turchanin, X. Feng, K. Müllen, *Adv. Mater.* 24 (2012) 5130-5135.

[105] Engineering, Least Dense 3D-Printed Graphene Structure Enabled by New Technique. http://www.engineering.com/3DPrinting/3DPrintingArticles/ArticleID/15209/Least-

Dense-3D-Printed-Graphene-Structure-Enabled-by-New-Technique.aspx, 2017(accessed 17.08.03).

[106] D. Lin, S. Jin, F. Zhang, C. Wang, Y. Wang, C. Zhou, G. J. Cheng, *Nanotechnology* 26 (2015) 434003.

[107] Z. C. Eckel, C. Zhou, J. H. Martin, A. J. Jacobsen, W. B. Carter, T. A. Schaedler, *Science* 351 (2016) 58-62.

[108] J. Lin, C. Zhang, Z. Yan, Y. Zhu, Z. Peng, R. H. Hauge, D. Natelson, J. M. Tour, *Nano Lett.* 13 (2012) 72-78.

[109] Z. Niu, L. Zhang, L. Liu, B. Zhu, H. Dong, X. Chen, *Adv. Mater.* 25 (2013) 4035-4042.

[110] C. Wang, L. Taherabadi, G. Jia, M. Madou, Y. Yeh, B. Dunn, *Electrochem. Solid-State Lett.* 7 (2004) A435-A438.

[111] J. Czyżewski, P. Burzyński, K. Gaweł, J. Meisner, *J. Mater. Process. Technol.* 209 (2009) 5281-5285.

[112] B. Xu, X.-y. Wu, J.-g. Lei, R. Cheng, S.-c. Ruan, Z.-l. Wang, *Int. J. Adv. Manuf. Tech.* 80 (2015) 1701-1711.

[113] N. A. Kyerematen, T. Brousse, D. Pech, *Nat. Nanotechnol.* 12 (2017) 7-15.

[114] D. Miranda, C. Costa, A. Almeida, S. Lanceros-Méndez, *J. Electroanal. Chem.* 780 (2016) 1-11.

[115] J. Park, J. Li, W. Lu, A. Sastry, *J. Appl. Phys.* 119 (2016)p. 025101.

[116] C. L. Cobb, C. C. Ho, *Electrochem. Soc. Interface* 25 (2016) 75-78.

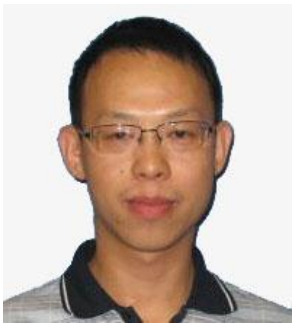

Feng Zhang is a Ph.D. candidate at University at Buffalo (UB), SUNY. He received his Bachelor degree from Wuhan University of Technology in 2005. After several years' experience in industry, he attended UB and received his master degree in Industrial and Systems Engineering in 2014. His current research interests include developing novel 3D printing methods for fabrication of various porous materials.

Min Wei received his Bachelor (2015) and Master (2017) degrees of Chemical Engineering from the University at Buffalo (UB), SUNY. His research in Professor Gang Wu's group was to develop graphene-like carbon materials for electrochemical energy storage applications, especially for supercapacitor and Lithium air battery.

Vilayanur Viswanathan is a Senior Engineer at Pacific Northwest National Laboratory. He received his BS in Chemical Engineering from the Indian Institute of Technology, Madras, and Ph.D. from Rutgers University in Chemical and Electrochemical Engineering. His research focus areas are cost performance modeling of large scale battery systems, battery state of health modeling, and development of test protocols, testing & analysis for grid scale energy storage. He is a Keystone Task Leader for Cell Design and Integration for the Batt 500 program, and is

the Technical Advisor to the US Technical Advisory Group to IEC TC120 to develop standards for electrical energy storage systems.

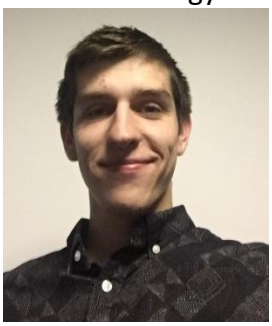

Benjamin Swart is studying for his Bachelors of Science degree in Industrial Engineering at the University at Buffalo. His research work consists of additive manufacturing (3D printing) on a macro scale, product design, computer aided design (CAD), and new prototyping methods.

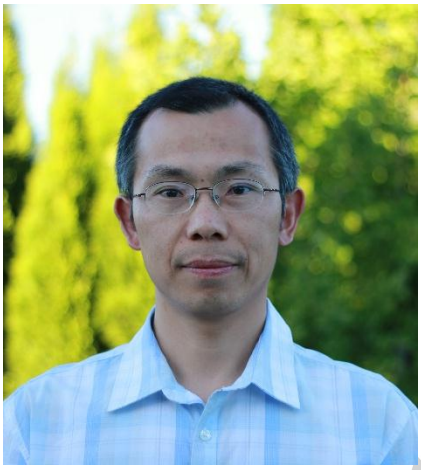

Yuyan Shao (Ph.D.) is a Senior Scientist at Pacific Northwest National Laboratory. His research focus is on electrochemical materials and systems for energy storage and conversion. He has published over 100 papers with 12000+ citations (H Index=49). He is an inventor on over 30 patents/patent applications. He was awarded Thomson-Reuters Highly Cited Researcher. He also serves as an Editorial Board Member for Scientific Reports, a guest editor for Nano Energy Electrocatalysis Special Issue.

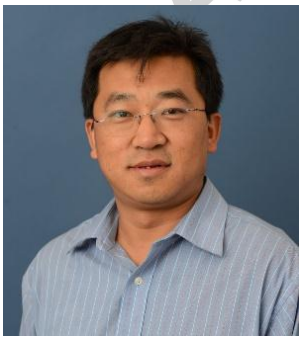

Gang Wu is an Assistant Professor in the Department of Chemical and Biological Engineering at the University at Buffalo (SUNY-Buffalo). He completed his Ph.D. studies at the Harbin Institute of Technology in 2004 followed by extensive postdoctoral trainings at

Tsinghua University (2004-2006), the University of South Carolina (2006-2008), and Los Alamos National Laboratory (LANL) (2008-2010). Then he was a staff scientist at LANL until he joined SUNY-Buffalo in 2014. His research focuses on functional materials and catalysts for electrochemical energy storage and conversion. He has written more than 150 papers with a citation of >10,000 times.

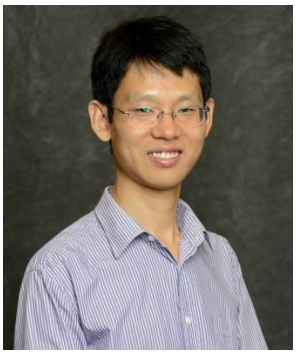

Chi Zhou is an assistant professor in Department of Industrial and Systems Engineering at the University at Buffalo. He received his Ph.D. degree in Industrial and Systems Engineering from the University of Southern California (USC) in 2012 and his master's degree in Computer Science from USC in 2010. Prior to joining UB in July 2013, Zhou was a senior research and development engineer at EnvisionTec Inc. Dr. Zhou's current research focuses on additive manufacturing (3D printing) process modeling and optimization for advanced materials including nano- and bio- materials.

Highlights

• The advantages of utilizing 3D printing technologies to fabricate EES devices are highlighted.

• An overview of employing 3D printing processes in EES area are provided.

• Materials criteria using 3D printing processes assembly is herein discussed.

• A mapping of materials and processes with EES conventional fabrication approaches and 3D printing approaches are built.

Graphic abstract: